



Throw Light on the Heavy Economic Minerals of the Northern Part of Delta, Egypt

¹El Afandy A., ²Khalil M., ¹El Azab A., ¹El Alfi S., ¹Etman M. and H.R. Saad²

¹Nuclear Materials Authority, Cairo, Egypt.

²Faculty of Science, Damietta University, Egypt.

Received: 11 Sept. 2022

Accepted: 19 Oct. 2022

Published: 15 Dec. 2022

ABSTRACT

The studied area extended from Rashid branch to the Dumyat branch, the area has a long reach to 150 km, and the area width reach to 2km. The collected samples were acquired by using spiral bar manually rotating for one meter depth. The samples were distributed along 30 profiles perpendicular to the beach, and the distance between them are about 4.5 to 5 km. Each profile includes three samples representing different environments present at such profile. The distance between the samples along each profile ranging from 200 to 750 m perpendicular to the shore line. These samples analyses in the nuclear materials authority labs, and study the samples under stereo-binocular microscope. The area has average total heavy mineral (9.7%), and average of economic heavy minerals (2.8). The average percentage of Magnetite (0.58%), Ilmenite (1.4%), Garnet (0.21%), Rutile (0.05%), Leucoxene (0.15%), Zircon (0.14%), Monazite (0.005%), and Sphene (0.01%). The economic heavy minerals concentrated in the central part of the study area where these sediments are related to the old extinct river branches; Canopic, Sebbyntic, and Bucoloic. The area under study is very economic important.

Keywords: Rashid and Dumyat branch, spiral bar manually, heavy economic minerals, profiles

1. Introduction

The river Nile is the second longest river in the world, its length reaches about 6500 km from its sources in Central Africa to its outlets in the Mediterranean Sea.

Its waters drifted from two main sources: the Abyssinian Plateau and the northern Lake Region of the Central African Plateau. This water carries huge amounts of deposits derived from the denudation of all igneous and metamorphic rocks. Most of these deposits are including heavy economic minerals. The rich placer deposits of heavy economic minerals have been deposited along the northern beaches on the delta coast.

These sediments are pushed towards the beaches and the submerged offshore sandbars by displacement in suspension and saltation. Through this phase of transportation under the seawater in the shelf area, the grains undergo an effective action of sorting (Hammoud, 1973). The subsequent wind action transports, some of these sediments accumulated as sand dunes along the beach (Sadek *et al.*, 1988). Heavy minerals occurred mainly in the aeolian sand dune belts, that outcropping at Maestro, El Burullus, Baltim, and Gamsa.

According to Kuenan (1962), the Nile River carries about million m³ of sediments to the Mediterranean Sea every year. The solid matter constitutes about 15-45% of the sand fractions; the rest are silt and clay. This enormous quantity of sediments has been outpoured through the present Rashid and Dumyat mouths, as well as through the outpourings of the seven old extent Nile branches during the last century (Ball, 1942).

Extensive black sands placer deposits are discontinuously distributed along the northern Mediterranean coastal plain of the Nile Delta as well as Sinai Peninsula. These areas were originally investigated by many authors as: Dabbour (1994, 1997 and 1999) Rabie *et al.*, (1995), El hadary (1998), El-rakaiby (2000), Abu Diab (2002), Ali *et al.*, (2003), El Balakssy (2003), El Azab (2006), Moustafa

(2010), Samy and El-Gohary (2013), Rajab *et al.*, (2017), El Azab *et al.*, (2018, and 2019), Shousha *et al.*, (2019) and El Alfi (2019).

El Rakaiby and Attia (2004) studied and divided the northern coast from El Salum to Rafah into three coasts of different geological, structure and morphological features. They are the western rocky coast, the central muddy or delta coast, and the eastern sandy coast. The study area belonging to the muddy coasts.

In the light of these data, the Nuclear Materials Authority has established a plant for the exploitation of the Egyptian placer deposits at Rashid area to produce monazite, zircon, and rutile concentrates. The studied area limited between Rashid branch and Dumyat branch on the Mediterranean Sea (Fig. 1). The Rashid branch receives today most of the water of the Nile as it has less meandered and more bifurcates into the Delta fan compared with Dumyat branch. The Nile Delta coast and Nile branches in classical time are shown in figure (2) after Wiegell (2009).

Brief of geomorphology and environment of the north delta coast

The northern Egyptian shoreline extends from Rafah at the east to El Salom at the west. According to El Rakaiby and Attia (2004) the northern coast can be divided into three coasts possesses different morphological forms and geological units as follow:

- 1-The sandy or Sinai coast (eastern coast) extends from Rafah to Romana.
 - 2-The muddy or Delta coast (central coast) extends from Romana to El Dikhela.
 - 3-The rocky or the north western desert coast (western coast) extends from El Dikhela to El Salom.
- This study is mainly concerned to the second coastal divisions (muddy coasts).

Geomorphological Units of the Coast

The coast is formally defined as the geographical upland region adjacent to a sea. The study coastal environment includes the following morphological units:

- 1-Beach (Shore), which is the strip of ground bordering any body of water, over with the beach sands actively oscillate with changing wave action.
- 2-Coastal plain made up of fine and very fine sand with limited patches of medium and coarse sand.
- 3-Coastal dunes, they are mainly represented by belts of fine and very fine sand, usually located at the southern margins of the beach extending parallel to the coastal line.
- 4-Coastal lakes; it is a part of low land received the fresh water from the river and the sea nearest it, represented in the study area by El Burullus.
- 5-Coastal Sabkhas, which represented by low laying lands composed mainly of mud, silt and sand. They are mostly wet and salty, and located mainly in the coastal plain extended, parallel to the shore and around lakes as well as the lowest relief areas.

The coastal environment is the area lying at the interface between the land and the sea. As in other geomorphic environments, coastal areas are composed of a wide range of landforms. The coastal environment includes both the zone of shallow water within which waves are able to move sediment, and the area land-ward of this zone, including beaches, coastal plains, coastal dunes, lakes, water bodies and sabkha areas. These landforms are affected to some degree by the direct or indirect effects of marine waves, tides and currents. The length of coastal environment of the study area is extended for about 156 kilometers, and formed of the delta or muddy coast (El Rakaiby and Attia, 2004).

Water in Mediterranean Sea is in constant motion as the other oceans of the world. It moves by wind generated waves, tides, and a variety of currents. It constantly modifies the shores, reshaping coastlines with less activity of waves and currents. The Delta beaches are composed of unconsolidated and readily transportable sand, occasionally, they can adjust quickly to changes in the nature and energy of coastal processes.

The Holocene has been great changes in the position of shorelines and in coastal morphology as a result of predominantly rising sea levels (Summerfield, 1991).

Shoreline processes can change in intensity from day to day, and from season to season but they never stop. According to Keller, (2000), winds generated waves period most of the energy for shoreline processes. The refraction waves concentrate energy on headlands (such as Rashid and Domiat heads). One of the most important shoreline processes is the long-shore drift current which generates by waves advancing obliquely lowland the shore.

In general, the Delta shorelines are especially important because they include economic minerals deposited associated with their beach sands, as well as the concentration of population on/or near the coasts.

The Mediterranean shore in front of the Nile Delta is nearly flat, narrow, and underline by fine to very fine sand. As the beginning of 20th century where low floods associated with deficiency in sediment load, the coast was changed from emerged to submerged and the progressive accretion has been changed at several places, into erosion of varying rates.

2. Method and Materials

Field Work (Samples)

The collected samples were acquired by using spiral bar manually rotating for one meter depth. The samples were distributed along 30 profiles perpendicular to the beach, and the distance between them are about 4.5 to 5 km. Each profile includes three samples representing different environments present at such profile. The distance between the samples along each profile ranging from 200 to 750 m perpendicular to the shore line. These samples are plotted on the Google Earth photo (Fig. 1), where the collected samples are 90 samples. Their weight of each collected sample is ranging from 10 to 15 kg. These samples transported to nuclear materials authority laboratory for treatment, and analyses.

Gravimetric Separation

The original sand samples were dried and passed from sieve 1mm to remove the shell, shell fragments, and the gravel (concretion of sand). The sample is quartered by John's splitters of different chutes until about 250gm, the rest sample was saved as reference sample.

A representative sub-sample weighting about 60gm was taken from each prepared sample by quartering for mineral separation. The gravimetric separation is used to separate the heavy minerals from the light minerals by using the heavy liquid bromoform with specific gravity of 2.86 g/cm³. This liquid separates between two minerals the first is lighter than these liquids and flow on it, and the second is heavier than these liquids and sink or fall or merged on it. The light fractions were discarded, while the heavy fraction used in further analysis. The magnetite separation carried out using a small hand magnet with suitable strength Table (1) (Flinter,1955).

Frantz Isodynamic Magnetic Separator were used to fractionate heavy minerals according to their magnetic susceptibilities (Model L-1). The free-magnetite samples were subjected to the magnetic separation at 0.2, 0.5, 1.0, 1.5 magnetic and 1.5 non-magnetic current amperes. Each fraction obtained from the magnetic separation process was microscopically studied under binocular stereomicroscope and investigated to calculate the frequency distribution of the concerned minerals in the samples.

The identified heavy mineral assemblages studied under a Binocular Stereomicroscope in the studied area can be classified into two main groups according to Folk (1980). The first one includes opaque minerals as; Magnetite, Hematite, Ilmenite, Leucoxene, and Pyrite. The second group comprises non-opaque minerals includes Garnet, Rutile, Titanite, Zircon, Monazite, Apatite. The less stable minerals compress Kyanite, Sillimanite, Andalusite, Epidote, Biotite, Muscovite and Green Silicates. The percentage of each mineral were calculated to the original samples also ranges and averages of the total heavy mineral for the studied sediments and tabulated in Table (2a, b and c).

Mineralogical investigation of the mineral constituents was carried out by Semi-quantitative EDX chemical analyses using a Phillips XL-30 Environmental Scanning Electron Microscope (ESEM) on individual grains of heavy minerals. The most important heavy minerals will be described in the following paragraphs:

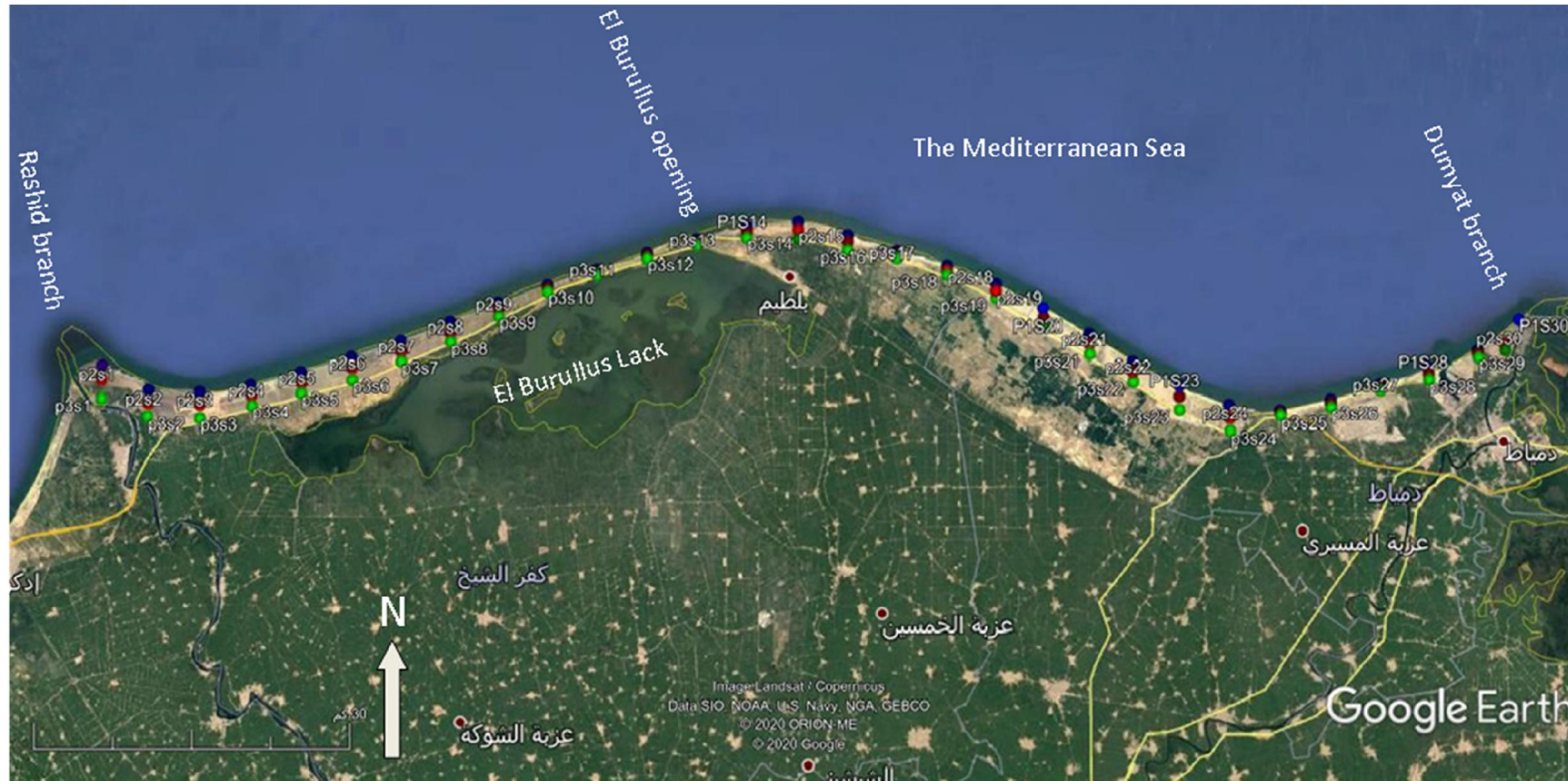


Fig. 1: Show samples locations on the Google Earth photo.

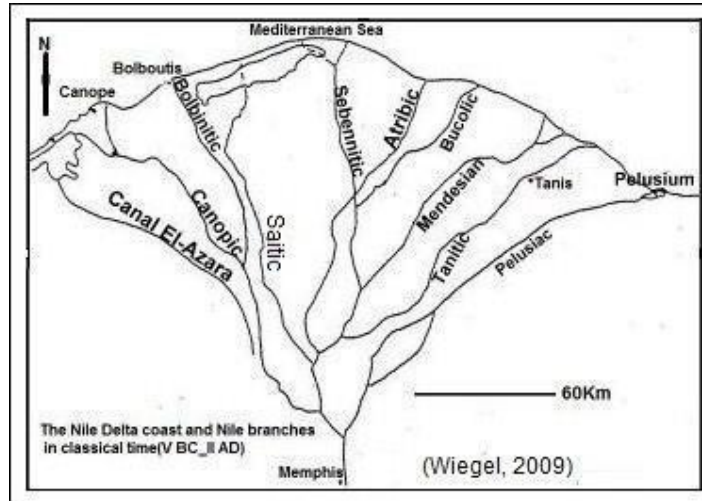


Fig. 2: The Nile Delta coast and Nile branches in classical time (V BC-II AD) (after Wiegel, 2009).

Table 1: Percentages of magnetite and total heavy bromoform for the studied area.

| So. No. | Line P1 | | So. No. | Line P2 | | So. No. | Line P3 | |
|---------|---------|--------|---------|---------|--------|---------|---------|--------|
| | Mgt. % | H.Br % | | Mgt. % | H.Br % | | Mgt. % | H.Br % |
| P1S1 | 1.790 | 26.620 | P2S1 | 0.930 | 15.460 | P3S1 | 1.740 | 25.490 |
| P1S2 | 1.770 | 18.870 | P2S2 | 1.220 | 18.290 | P3S2 | 1.650 | 19.470 |
| P1S3 | 1.320 | 15.370 | P2S3 | 1.380 | 16.260 | P3S3 | 1.109 | 9.581 |
| P1S4 | 1.120 | 9.200 | P2S4 | 0.845 | 9.205 | P3S4 | 0.983 | 9.207 |
| P1S5 | 1.100 | 7.020 | P2S5 | 0.714 | 6.116 | P3S5 | 0.880 | 6.820 |
| P1S6 | 1.076 | 6.416 | P2S6 | 0.684 | 4.403 | P3S6 | 0.784 | 6.203 |
| P1S7 | 0.964 | 6.827 | P2S7 | 0.255 | 2.030 | P3S7 | 0.647 | 4.238 |
| P1S8 | 0.952 | 4.487 | P2S8 | 0.534 | 2.746 | P3S8 | 0.087 | 4.183 |
| P1S9 | 0.634 | 3.077 | P2S9 | 0.359 | 2.977 | P3S9 | 0.069 | 3.491 |
| P1S10 | 0.582 | 2.888 | P2S10 | 0.333 | 2.877 | P3S10 | 0.065 | 3.365 |
| P1S11 | 0.565 | 2.775 | P2S11 | 0.328 | 2.742 | P3S11 | 0.059 | 3.181 |
| P1S12 | 0.560 | 2.720 | P2S12 | 0.306 | 2.634 | P3S12 | 0.054 | 3.136 |
| P1S13 | 0.112 | 16.211 | P2S13 | 0.968 | 14.052 | P3S13 | 0.979 | 13.321 |
| P1S14 | 1.197 | 54.700 | P2S14 | 1.623 | 46.887 | P3S14 | 1.348 | 34.292 |
| P1S15 | 0.694 | 26.404 | P2S15 | 1.157 | 23.023 | P3S15 | 1.272 | 21.798 |
| P1S16 | 0.246 | 17.089 | P2S16 | 0.973 | 15.557 | P3S16 | 0.984 | 13.296 |
| P1S17 | 0.189 | 14.271 | P2S17 | 0.845 | 11.885 | P3S17 | 0.712 | 10.468 |
| P1S18 | 0.347 | 15.311 | P2S18 | 0.863 | 12.557 | P3S18 | 0.731 | 11.489 |
| P1S19 | 0.114 | 13.435 | P2S19 | 0.858 | 12.262 | P3S19 | 0.726 | 10.994 |
| P1S20 | 0.123 | 8.545 | P2S20 | 0.443 | 6.367 | P3S20 | 0.493 | 4.907 |
| P1S21 | 0.095 | 7.136 | P2S21 | 0.427 | 5.653 | P3S21 | 0.486 | 4.644 |
| P1S22 | 0.215 | 8.150 | P2S22 | 0.411 | 4.919 | P3S22 | 0.427 | 4.203 |
| P1S23 | 0.129 | 7.632 | P2S23 | 0.403 | 4.577 | P3S23 | 0.391 | 3.779 |
| P1S24 | 0.119 | 7.503 | P2S24 | 0.392 | 4.118 | P3S24 | 0.352 | 3.488 |
| P1S25 | 0.094 | 6.238 | P2S25 | 0.371 | 3.739 | P3S25 | 0.328 | 2.812 |
| P1S26 | 0.079 | 5.642 | P2S26 | 0.343 | 3.507 | P3S26 | 0.304 | 2.626 |
| P1S27 | 0.026 | 1.538 | P2S27 | 0.215 | 0.915 | P3S27 | 0.117 | 0.963 |
| P1S28 | 0.024 | 1.512 | P2S28 | 0.126 | 0.924 | P3S28 | 0.100 | 0.920 |
| P1S29 | 0.019 | 1.257 | P2S29 | 0.051 | 0.879 | P3S29 | 0.078 | 0.832 |
| P1S30 | 0.016 | 1.137 | P2S30 | 0.011 | 0.759 | P3S30 | 0.041 | 0.649 |
| Min. | 0.016 | 1.137 | Min. | 0.011 | 0.759 | Min. | 0.041 | 0.649 |
| Max. | 1.790 | 54.700 | Max. | 1.623 | 46.887 | Max. | 1.740 | 34.292 |
| Aveg. | 0.542 | 10.666 | Aveg. | 0.612 | 8.611 | Aveg. | 0.600 | 8.128 |

Table 2a: The percentage of Heavy Economic Minerals in studied samples for line P1.

| So. No. | mag. | ilm. | leuco. | gar. | Zir. | Rut. | Mon. | sph. | T.E.M | G.S | Total |
|---------|-------|-------|--------|-------|-------|-------|--------|--------|--------|--------|--------|
| P1S1 | 1.790 | 3.010 | 0.150 | 0.230 | 0.230 | 0.080 | 0.0090 | 0.0150 | 5.514 | 22.896 | 28.410 |
| P1S2 | 1.770 | 2.820 | 0.139 | 0.200 | 0.190 | 0.060 | 0.0080 | 0.0130 | 5.200 | 15.440 | 20.640 |
| P1S3 | 1.320 | 2.310 | 0.112 | 0.160 | 0.160 | 0.050 | 0.0070 | 0.0110 | 4.130 | 12.560 | 16.690 |
| P1S4 | 1.120 | 2.130 | 0.094 | 0.110 | 0.120 | 0.020 | 0.0050 | 0.0060 | 3.605 | 6.715 | 10.320 |
| P1S5 | 1.100 | 2.070 | 0.080 | 0.120 | 0.110 | 0.040 | 0.0050 | 0.0070 | 3.532 | 4.588 | 8.120 |
| P1S6 | 1.076 | 1.978 | 0.138 | 0.154 | 0.112 | 0.075 | 0.0070 | 0.0120 | 3.552 | 3.940 | 7.492 |
| P1S7 | 0.964 | 1.968 | 0.110 | 0.162 | 0.113 | 0.104 | 0.0070 | 0.0050 | 3.433 | 4.358 | 7.791 |
| P1S8 | 0.952 | 1.648 | 0.083 | 0.259 | 0.110 | 0.080 | 0.0060 | 0.0100 | 3.148 | 2.291 | 5.439 |
| P1S9 | 0.634 | 0.982 | 0.080 | 0.084 | 0.098 | 0.040 | 0.0050 | 0.0040 | 1.927 | 1.784 | 3.711 |
| P1S10 | 0.582 | 0.974 | 0.080 | 0.079 | 0.094 | 0.039 | 0.0049 | 0.0030 | 1.856 | 1.614 | 3.470 |
| P1S11 | 0.565 | 0.968 | 0.076 | 0.073 | 0.091 | 0.036 | 0.0048 | 0.0030 | 1.817 | 1.523 | 3.340 |
| P1S12 | 0.560 | 0.962 | 0.073 | 0.070 | 0.089 | 0.035 | 0.0047 | 0.0040 | 1.798 | 1.482 | 3.280 |
| P1S13 | 0.112 | 4.500 | 0.413 | 0.835 | 0.403 | 0.153 | 0.0080 | 0.0090 | 6.433 | 9.890 | 16.323 |
| P1S14 | 1.197 | 7.534 | 1.094 | 2.408 | 0.752 | 0.326 | 0.0130 | 0.0600 | 13.384 | 42.513 | 55.897 |
| P1S15 | 0.694 | 5.874 | 1.068 | 2.505 | 0.445 | 0.260 | 0.0090 | 0.0500 | 10.905 | 16.193 | 27.098 |
| P1S16 | 0.246 | 1.941 | 0.202 | 0.722 | 0.172 | 0.075 | 0.0070 | 0.0020 | 3.367 | 13.968 | 17.335 |
| P1S17 | 0.189 | 1.732 | 0.171 | 0.513 | 0.142 | 0.053 | 0.0060 | 0.0010 | 2.807 | 11.653 | 14.460 |
| P1S18 | 0.347 | 2.937 | 0.534 | 1.253 | 0.223 | 0.130 | 0.0060 | 0.0250 | 5.455 | 10.203 | 15.658 |
| P1S19 | 0.114 | 2.032 | 0.183 | 0.536 | 0.169 | 0.054 | 0.0025 | 0.0010 | 3.092 | 10.458 | 13.549 |
| P1S20 | 0.123 | 0.971 | 0.101 | 0.361 | 0.086 | 0.038 | 0.0020 | 0.0010 | 1.682 | 6.986 | 8.668 |
| P1S21 | 0.095 | 0.866 | 0.086 | 0.257 | 0.071 | 0.027 | 0.0018 | 0.0005 | 1.402 | 5.828 | 7.230 |
| P1S22 | 0.215 | 1.822 | 0.331 | 0.777 | 0.138 | 0.081 | 0.0019 | 0.0155 | 3.382 | 4.983 | 8.365 |
| P1S23 | 0.129 | 1.384 | 0.457 | 0.442 | 0.079 | 0.020 | 0.0004 | 0.0037 | 2.515 | 5.246 | 7.761 |
| P1S24 | 0.119 | 1.345 | 0.412 | 0.407 | 0.065 | 0.010 | 0.0004 | 0.0050 | 2.362 | 5.260 | 7.622 |
| P1S25 | 0.094 | 1.255 | 0.352 | 0.342 | 0.045 | 0.010 | 0.0002 | 0.0025 | 2.102 | 4.230 | 6.332 |
| P1S26 | 0.079 | 1.062 | 0.258 | 0.203 | 0.025 | 0.005 | 0.0002 | 0.0037 | 1.637 | 4.084 | 5.721 |
| P1S27 | 0.026 | 0.279 | 0.092 | 0.098 | 0.016 | 0.004 | 0.0001 | 0.0010 | 0.516 | 1.048 | 1.564 |
| P1S28 | 0.024 | 0.271 | 0.083 | 0.082 | 0.013 | 0.002 | 0.0000 | 0.0000 | 0.475 | 1.061 | 1.536 |
| P1S29 | 0.019 | 0.253 | 0.071 | 0.069 | 0.009 | 0.002 | 0.0001 | 0.0010 | 0.424 | 0.852 | 1.276 |
| P1S30 | 0.016 | 0.214 | 0.052 | 0.041 | 0.005 | 0.001 | 0.0001 | 0.0010 | 0.330 | 0.823 | 1.153 |
| Min. | 0.016 | 0.214 | 0.052 | 0.041 | 0.005 | 0.001 | 0.0000 | 0.0000 | 0.330 | 0.823 | 1.153 |
| Max. | 1.790 | 7.534 | 1.094 | 2.505 | 0.752 | 0.326 | 0.0130 | 0.0600 | 13.384 | 42.513 | 55.897 |
| Aveg. | 0.542 | 1.936 | 0.239 | 0.452 | 0.146 | 0.064 | 0.0044 | 0.0092 | 3.393 | 7.816 | 11.208 |

Table 2b: The percentage of Heavy Economic Minerals in studied samples for line P2.

| So. No. | mag. | ilm. | leuco. | gar. | Zir. | Rut. | Mon. | sph. | T.E.M | G.S | Total |
|---------|-------|-------|--------|-------|-------|-------|--------|--------|-------|--------|--------|
| P2S1 | 0.930 | 2.113 | 0.122 | 0.219 | 0.225 | 0.066 | 0.0110 | 0.0160 | 3.702 | 12.688 | 16.390 |
| P2S2 | 1.220 | 2.325 | 0.134 | 0.224 | 0.236 | 0.073 | 0.0120 | 0.0190 | 4.243 | 15.267 | 19.510 |
| P2S3 | 1.380 | 2.267 | 0.130 | 0.203 | 0.185 | 0.068 | 0.0110 | 0.0180 | 4.262 | 13.378 | 17.640 |
| P2S4 | 0.845 | 1.853 | 0.091 | 0.134 | 0.117 | 0.051 | 0.0090 | 0.0150 | 3.115 | 6.935 | 10.050 |
| P2S5 | 0.714 | 1.546 | 0.083 | 0.096 | 0.091 | 0.047 | 0.0070 | 0.0100 | 2.594 | 4.236 | 6.830 |
| P2S6 | 0.684 | 1.045 | 0.057 | 0.087 | 0.074 | 0.036 | 0.0060 | 0.0070 | 1.996 | 3.091 | 5.087 |
| P2S7 | 0.255 | 0.567 | 0.007 | 0.065 | 0.052 | 0.049 | 0.0050 | 0.0050 | 1.005 | 1.280 | 2.285 |
| P2S8 | 0.534 | 0.988 | 0.075 | 0.098 | 0.067 | 0.025 | 0.0070 | 0.0070 | 1.801 | 1.479 | 3.280 |
| P2S9 | 0.359 | 0.876 | 0.074 | 0.099 | 0.051 | 0.012 | 0.0040 | 0.0040 | 1.479 | 1.857 | 3.336 |
| P2S10 | 0.333 | 0.841 | 0.073 | 0.094 | 0.048 | 0.011 | 0.0040 | 0.0050 | 1.409 | 1.801 | 3.210 |
| P2S11 | 0.328 | 0.835 | 0.069 | 0.086 | 0.047 | 0.009 | 0.0040 | 0.0040 | 1.382 | 1.688 | 3.070 |
| P2S12 | 0.306 | 0.811 | 0.062 | 0.083 | 0.018 | 0.006 | 0.0030 | 0.0040 | 1.293 | 1.647 | 2.940 |
| P2S13 | 0.968 | 2.463 | 0.343 | 0.325 | 0.213 | 0.054 | 0.0090 | 0.0130 | 4.388 | 10.632 | 15.020 |
| P2S14 | 1.623 | 5.517 | 0.718 | 0.814 | 0.623 | 0.283 | 0.0190 | 0.0240 | 9.621 | 38.889 | 48.510 |
| P2S15 | 1.157 | 3.691 | 0.665 | 0.632 | 0.536 | 0.237 | 0.0130 | 0.0210 | 6.952 | 17.228 | 24.180 |
| P2S16 | 0.973 | 1.986 | 0.473 | 0.611 | 0.519 | 0.199 | 0.0110 | 0.0190 | 4.791 | 11.739 | 16.530 |
| P2S17 | 0.845 | 1.675 | 0.368 | 0.371 | 0.326 | 0.151 | 0.0090 | 0.0130 | 3.758 | 8.972 | 12.730 |
| P2S18 | 0.863 | 1.798 | 0.399 | 0.403 | 0.397 | 0.168 | 0.0100 | 0.0150 | 4.053 | 9.367 | 13.420 |
| P2S19 | 0.858 | 1.572 | 0.374 | 0.382 | 0.346 | 0.165 | 0.0090 | 0.0140 | 3.720 | 9.400 | 13.120 |
| P2S20 | 0.443 | 0.955 | 0.100 | 0.225 | 0.211 | 0.115 | 0.0070 | 0.0090 | 2.065 | 4.745 | 6.810 |
| P2S21 | 0.427 | 0.860 | 0.079 | 0.132 | 0.130 | 0.099 | 0.0060 | 0.0090 | 1.742 | 4.338 | 6.080 |
| P2S22 | 0.411 | 0.827 | 0.078 | 0.093 | 0.080 | 0.071 | 0.0060 | 0.0080 | 1.574 | 3.756 | 5.330 |
| P2S23 | 0.403 | 0.813 | 0.071 | 0.087 | 0.079 | 0.070 | 0.0050 | 0.0070 | 1.535 | 3.445 | 4.980 |
| P2S24 | 0.392 | 0.784 | 0.065 | 0.081 | 0.073 | 0.068 | 0.0030 | 0.0060 | 1.472 | 3.038 | 4.510 |
| P2S25 | 0.371 | 0.780 | 0.063 | 0.063 | 0.060 | 0.056 | 0.0020 | 0.0050 | 1.400 | 2.710 | 4.110 |
| P2S26 | 0.343 | 0.755 | 0.060 | 0.062 | 0.057 | 0.051 | 0.0020 | 0.0040 | 1.334 | 2.516 | 3.850 |
| P2S27 | 0.215 | 0.290 | 0.041 | 0.045 | 0.040 | 0.034 | 0.0010 | 0.0020 | 0.668 | 0.462 | 1.130 |
| P2S28 | 0.126 | 0.264 | 0.039 | 0.041 | 0.038 | 0.021 | 0.0010 | 0.0020 | 0.532 | 0.518 | 1.050 |
| P2S29 | 0.051 | 0.258 | 0.028 | 0.033 | 0.031 | 0.019 | 0.0010 | 0.0020 | 0.423 | 0.507 | 0.930 |
| P2S30 | 0.011 | 0.241 | 0.018 | 0.011 | 0.009 | 0.001 | 0.0010 | 0.0010 | 0.293 | 0.477 | 0.770 |
| Min. | 0.011 | 0.241 | 0.007 | 0.011 | 0.009 | 0.001 | 0.001 | 0.001 | 0.293 | 0.462 | 0.770 |
| Max. | 1.623 | 5.517 | 0.718 | 0.814 | 0.623 | 0.283 | 0.019 | 0.024 | 9.621 | 38.889 | 48.510 |
| Aveg. | 0.612 | 1.387 | 0.165 | 0.197 | 0.166 | 0.077 | 0.007 | 0.010 | 2.620 | 6.603 | 9.223 |

Table 2c: The percentage of Heavy Economic Minerals in studied samples for line P3.

| So. No. | mag. | ilm. | leuco. | gar. | Zir. | Rut. | Mon. | sph. | T.E.M | G.S | Total |
|---------|-------|-------|--------|-------|-------|-------|--------|--------|-------|--------|--------|
| P3S1 | 1.740 | 2.915 | 0.135 | 0.318 | 0.240 | 0.094 | 0.0130 | 0.0150 | 5.470 | 21.760 | 27.230 |
| P3S2 | 1.650 | 2.283 | 0.118 | 0.273 | 0.213 | 0.085 | 0.0100 | 0.0130 | 4.645 | 16.475 | 21.120 |
| P3S3 | 1.109 | 1.974 | 0.099 | 0.130 | 0.109 | 0.063 | 0.0090 | 0.0120 | 3.505 | 7.185 | 10.690 |
| P3S4 | 0.983 | 1.944 | 0.095 | 0.128 | 0.098 | 0.061 | 0.0090 | 0.0110 | 3.329 | 6.861 | 10.190 |
| P3S5 | 0.880 | 1.721 | 0.086 | 0.113 | 0.088 | 0.052 | 0.0080 | 0.0110 | 2.959 | 4.741 | 7.700 |
| P3S6 | 0.784 | 1.652 | 0.075 | 0.103 | 0.076 | 0.041 | 0.0080 | 0.0080 | 2.747 | 4.240 | 6.987 |
| P3S7 | 0.647 | 1.323 | 0.064 | 0.088 | 0.064 | 0.027 | 0.0060 | 0.0070 | 2.226 | 2.659 | 4.885 |
| P3S8 | 0.087 | 0.312 | 0.031 | 0.065 | 0.041 | 0.005 | 0.0040 | 0.0030 | 0.548 | 3.722 | 4.270 |
| P3S9 | 0.069 | 0.348 | 0.033 | 0.107 | 0.043 | 0.006 | 0.0020 | 0.0040 | 0.612 | 2.948 | 3.560 |
| P3S10 | 0.065 | 0.340 | 0.032 | 0.063 | 0.041 | 0.006 | 0.0050 | 0.0060 | 0.558 | 2.872 | 3.430 |
| P3S11 | 0.059 | 0.331 | 0.031 | 0.060 | 0.037 | 0.005 | 0.0040 | 0.0050 | 0.532 | 2.708 | 3.240 |
| P3S12 | 0.054 | 0.308 | 0.028 | 0.052 | 0.036 | 0.004 | 0.0040 | 0.0050 | 0.491 | 2.699 | 3.190 |
| P3S13 | 0.979 | 2.191 | 0.242 | 0.147 | 0.113 | 0.061 | 0.0080 | 0.0100 | 3.751 | 10.549 | 14.300 |
| P3S14 | 1.348 | 5.343 | 0.635 | 0.811 | 0.472 | 0.233 | 0.0140 | 0.0150 | 8.871 | 26.769 | 35.640 |
| P3S15 | 1.272 | 4.568 | 0.581 | 0.250 | 0.411 | 0.194 | 0.0110 | 0.0130 | 7.300 | 15.770 | 23.070 |
| P3S16 | 0.984 | 2.745 | 0.286 | 0.316 | 0.353 | 0.075 | 0.0070 | 0.0080 | 4.774 | 9.506 | 14.280 |
| P3S17 | 0.712 | 1.689 | 0.231 | 0.251 | 0.300 | 0.063 | 0.0060 | 0.0070 | 3.259 | 7.921 | 11.180 |
| P3S18 | 0.731 | 1.710 | 0.228 | 0.258 | 0.313 | 0.066 | 0.0070 | 0.0080 | 3.321 | 8.899 | 12.220 |
| P3S19 | 0.726 | 1.699 | 0.205 | 0.247 | 0.301 | 0.062 | 0.0060 | 0.0070 | 3.253 | 8.467 | 11.720 |
| P3S20 | 0.493 | 0.836 | 0.109 | 0.119 | 0.144 | 0.051 | 0.0060 | 0.0050 | 1.763 | 3.637 | 5.400 |
| P3S21 | 0.486 | 0.833 | 0.096 | 0.103 | 0.123 | 0.047 | 0.0040 | 0.0050 | 1.697 | 3.433 | 5.130 |
| P3S22 | 0.427 | 0.794 | 0.088 | 0.097 | 0.097 | 0.034 | 0.0030 | 0.0050 | 1.545 | 3.085 | 4.630 |
| P3S23 | 0.391 | 0.775 | 0.079 | 0.081 | 0.063 | 0.029 | 0.0030 | 0.0040 | 1.425 | 2.745 | 4.170 |
| P3S24 | 0.352 | 0.743 | 0.073 | 0.077 | 0.058 | 0.025 | 0.0030 | 0.0030 | 1.334 | 2.506 | 3.840 |
| P3S25 | 0.328 | 0.682 | 0.068 | 0.076 | 0.041 | 0.021 | 0.0030 | 0.0030 | 1.222 | 1.918 | 3.140 |
| P3S26 | 0.304 | 0.655 | 0.067 | 0.073 | 0.037 | 0.019 | 0.0020 | 0.0020 | 1.159 | 1.771 | 2.930 |
| P3S27 | 0.117 | 0.318 | 0.044 | 0.034 | 0.018 | 0.010 | 0.0010 | 0.0010 | 0.543 | 0.537 | 1.080 |
| P3S28 | 0.100 | 0.297 | 0.021 | 0.029 | 0.017 | 0.008 | 0.0010 | 0.0010 | 0.474 | 0.546 | 1.020 |
| P3S29 | 0.078 | 0.265 | 0.016 | 0.022 | 0.016 | 0.007 | 0.0010 | 0.0010 | 0.406 | 0.504 | 0.910 |
| P3S30 | 0.041 | 0.211 | 0.010 | 0.015 | 0.011 | 0.002 | 0.0010 | 0.0010 | 0.292 | 0.398 | 0.690 |
| Min. | 0.041 | 0.211 | 0.010 | 0.015 | 0.011 | 0.002 | 0.001 | 0.001 | 0.292 | 0.398 | 0.690 |
| Max. | 1.740 | 5.343 | 0.635 | 0.811 | 0.472 | 0.233 | 0.014 | 0.015 | 8.871 | 26.769 | 35.640 |
| Aveg. | 0.600 | 1.394 | 0.130 | 0.150 | 0.132 | 0.049 | 0.006 | 0.007 | 2.467 | 6.261 | 8.728 |

S.No.=Sample number, Mgt.=Magnetite, Ilm.=Ilmenite, Leuc.=leucoxene, Gar.=Garnet, Zr.=Zircon, Rut.=Rutile, Mon.=Monazite, Sph.= Sphene (titanite), T.E.M= Total Economic Mineral G.S.=Green silicates,

Microscopic Study

The opaque minerals

Magnetite (Fe₃O₄)

Magnetite is a ferromagnetic mineral with chemical composition ferrous-ferric oxide (Fe²⁺, Fe³⁺ O₄). It is a combination of Wustite (FeO, 31.03 wt.%) and hematite (Fe₂O₃, 68.97 wt.%). Deviation from theoretical proportion commonly takes place both during magmatic differentiation and weathering cycle.

Due to heterogeneous sources of the Egyptian black sand magnetite, it contains considerable amount of titanomagnetite in addition to small amounts of manganese, vanadium, and chromium rich varieties. The titanium free Magnetite forms only about 15 wt. % of the total Egyptian magnetite (Wassef and Mikhail, 1981).

Magnetite habit ranges from massive, granular, angular to sub-angular (Fig. 3a) and the octahedron crystals of magnetite are less frequent and occur as isolated grains or as parallel twins (Fig. 3b). Magnetite displays black to deep reddish-brown color, with metallic to dull luster. The brownish tint can be attributed to their alteration and/or oxidation process, in addition to the probable presence of exsolved ilmenite and/or hematite. Different types of magnetite-ilmenite intergrowths and their origin were studied previously by many workers (Basta 1972, Arafa 1990, Dewedar 1998, El Balakssy 2003, Hassaan 2005, Mansour 2009 and Barakat 2016).

In the first line (P1) magnetite display content range from 0.016% to 1.790% with an average of about 0.542%, while, in the second line (P2) range from 0.011% to 1.623% with an average of about 0.612% and in the third line (P3) range from 0.041% to 1.740% with an average of about 0.600%.

Picked pure magnetite grains were investigated under the Environmental Scanning Electronic Microscope (ESEM) and the elemental chemical compositions are shown in figure (3c), Titanomagnetite

magnetite contains up to 13% TiO₂ (Ward and Towner 1985) in the present study the EDX of magnetite (semi quantitative chemical analysis) shows additional weight percent of titanium reaches up to 16.83%. The titanomagnetite minerals such as magnetite, ilmenite, leucocoxene and rutile are mainly derived from the mafic volcanic rocks of the Blue Nile provenance beside gold traces (El-Kammar *et al.*, 2010). Pure magnetite grains were shown in figure (3d). The lateral distribution of magnetite percentages illustrated in (Fig. 4), and show the high concentration at the west and the middle parts While the low concentration located at the eastern part.

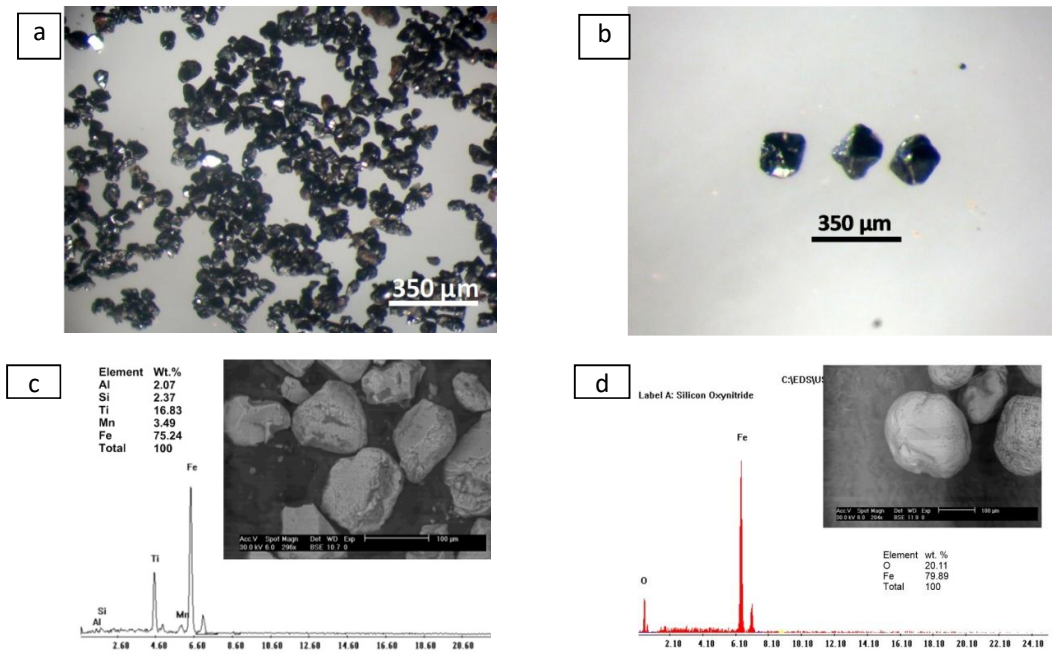


Fig. 3: Photomicrographs show: a) granular, angular to sub-angular magnetite, b) octahedron crystals of magnetite, c) EDX and BSE image of titanomagnetite grains and d) EDX and BSE image of magnetite grains.

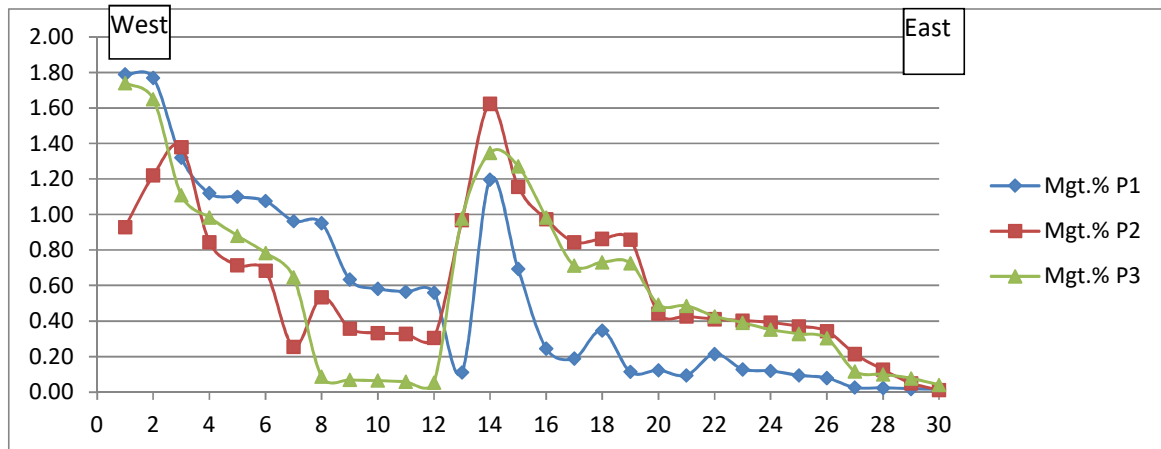


Fig. 4: lateral distribution of magnetite.

Hematite (Fe₂O₃)

Hematite is the principle ore of iron which originated mainly from magnetite alteration processes and alteration product of many Fe-bearing minerals especially pyrite and so called hematite after pyrite (goethite) or pseudomorphic pyrite. The non-crystalline forms of hematite are supposedly

transformations of the mineral limonite and occurs as a reddish brown to black color (Fig. 5a), as elongated rod like shape with red color angular to sub-angular with metallic or dull in earthy.

Pure hematite grains were investigated under the Environmental Scanning Electronic Microscope (ESEM) and the elemental chemical compositions are shown in figure (5b). It was recorded in all studied sediments as common accessory mineral.

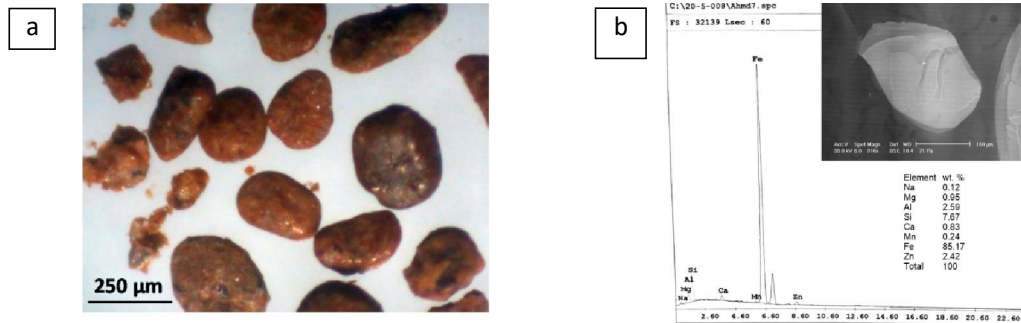


Fig. 5: Photomicrographs show: a) granular, angular to sub-angular hematite and b) EDX and BSE image of hematite grains

Ilmenite (FeO.TiO₂)

Ilmenite and their alteration product leucogene are processed for the production of titanium dioxide required for a high-quality white pigment used in paints, paper, plastics and cosmetics. Titanium dioxide white pigment is characterized by, high refractive index, high opacity, good reflectivity causes luminosity and whiteness, inertness and chemical stability (insoluble in acids, bases, organic solvents and air pollutants), none toxicity and high thermal stability.

Some ilmenite is used in sand blasting operations, in foundry moulds, and as a weighting agent in oil well drilling mud (El Bokel, 1984). Ground ilmenite can be used as a constituent of anti-corrosive paint substituting graphite. Ilmenite grains are also used as abrasive in petroleum industry for cleaning drill pipes and well pipes instead of silica.

Ilmenite was recorded as iron-black with metallic luster. It occurs as irregular angular to subangular with sharp edges (Fig. 6a) or with smooth edges, well rounded to subrounded (Fig. 6b), oval with smooth and pitted surface (Fig. 6c) and angular with strong striation (Fig. 6d) grains.

In the first line (P1) ilmenite display content range from 0.214% to 7.534% with an average of about 1.936%, while, in the second line (P2) range from 0.241% to 5.517% with an average of about 1.387% and in the third line (P3) range from 0.211% to 5.343% with an average of about 1.394%.

Pure ilmenite grains were investigated under the Environmental Scanning Electronic Microscope (ESEM) and the elemental chemical compositions are shown in figure (6e & f). The lateral distribution of ilmenite percentages illustrated in (Fig. 7), and show the high concentration at the central part and low concentration at the eastern part.

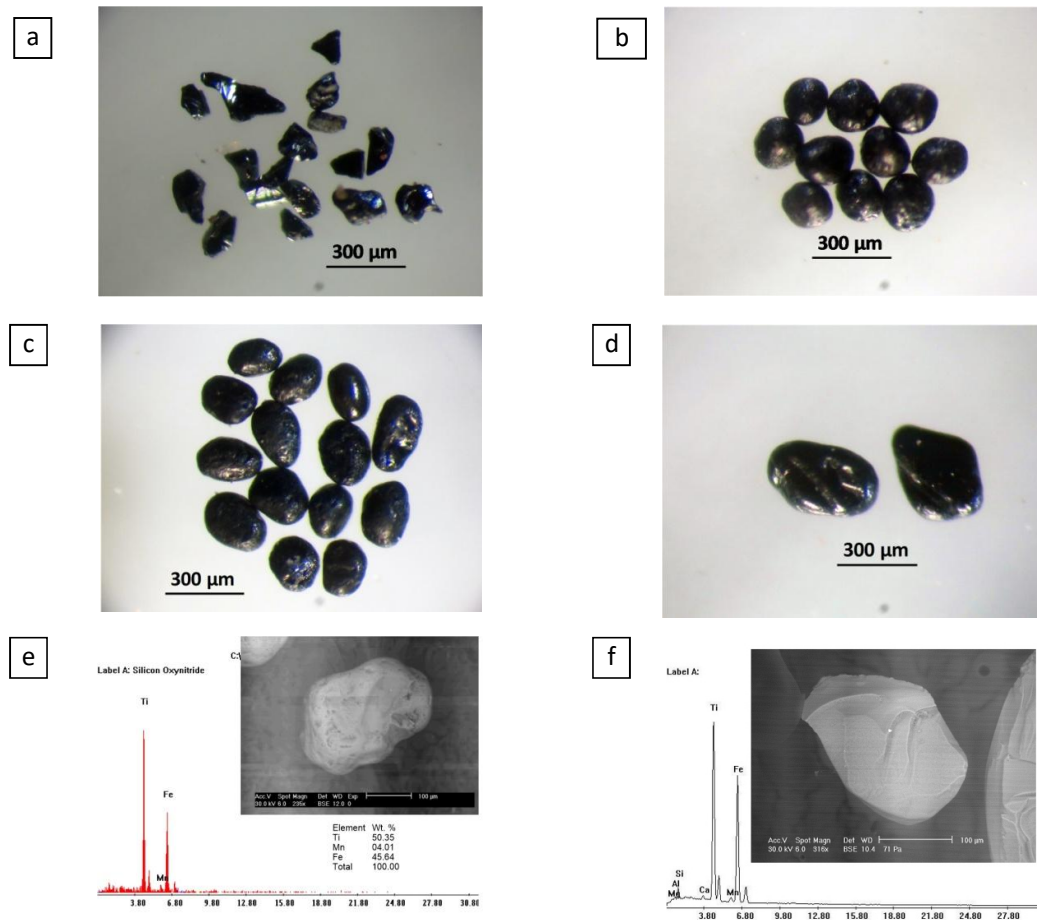


Fig. 6: photomicrograph shows: a) irregular ilmenite grains with sharp edges, b) rounded ilmenite grains, c) oval ilmenite grains, d) irregular ilmenite grains with strong striation and e & f) EDX and BSE image of ilmenite.

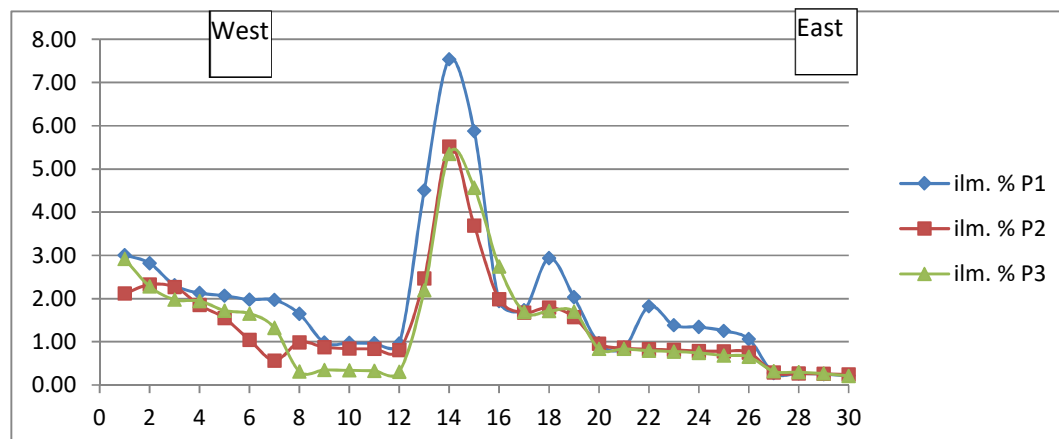


Fig. 7: lateral distribution of ilmenite.

Leucoxene

According to Bailey *et al.*, (1956), the alteration process of ilmenite is accompanied by change in their chemical and physical properties. Chemically the main results of alteration process are an increase in TiO_2 , Fe_2O_3 and H_2O and a decrease in FeO .

Teufer and Temple (1966) considered leucoxene as intermediate case between ilmenite and rutile called pseudo-rutile ($Fe_2Ti_3O_9$). The X-ray diffraction analysis showed that, the inter-planar d-spacing of pseudo-rutile are very close to those of ilmenite and rutile.

The leucoxene commonly occurs as rounded grains, opaque in transmitted light. A rough pitted surface is characteristic of most grains. The color of leucoxene grains from the Egyptian black sands varies from dark brown with black color represented remaining of ilmenite (Fig. 8a &b), white, brown to yellowish white (Fig. 8c &d). The color depends mainly on the degree of alteration (Mohamed, 1987, Mohamed, 1998 and Elsner, 2010). Ibrahim (1995) stated that, as the iron content decreases, the grain color becomes lighter brownish yellow, yellow, yellowish white and light creamy colors. Its specific gravity ranging from 3.5 to 4 according to the number of vugs formed in grains through iron withdrawal processes.

In the first line (P1) leucoxene display content range from 0.052% to 1.094% with an average of about 0.239%, while, in the second line (P2) range from 0.007% to 0.718% with an average of about 0.165% and in the third line (P3) range from 0.010% to 0.635% with an average of about 0.130%. The lateral distribution of leucoxene percentages illustrated in (Fig. 9), and show the high concentration at central part of the studied area.

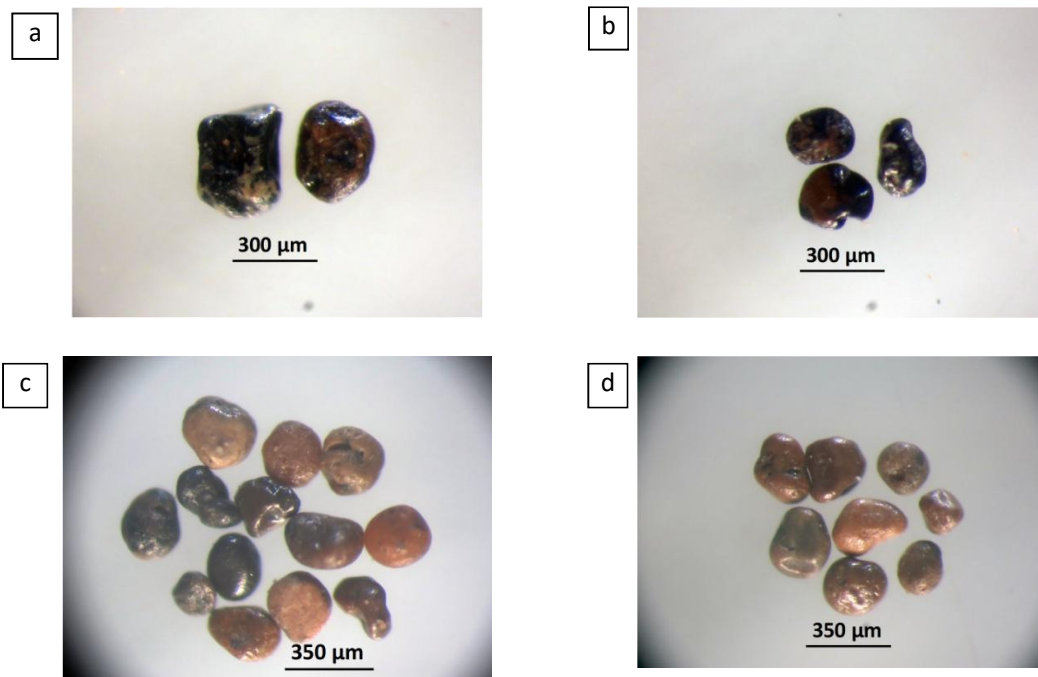


Fig. 8: Photomicrographs shows: a & b) dark brown and white leucoxene with black color remaining of ilmenite, c) Dark brown and brown color of leucoxene and d) Brown to light brown color of leucoxene.

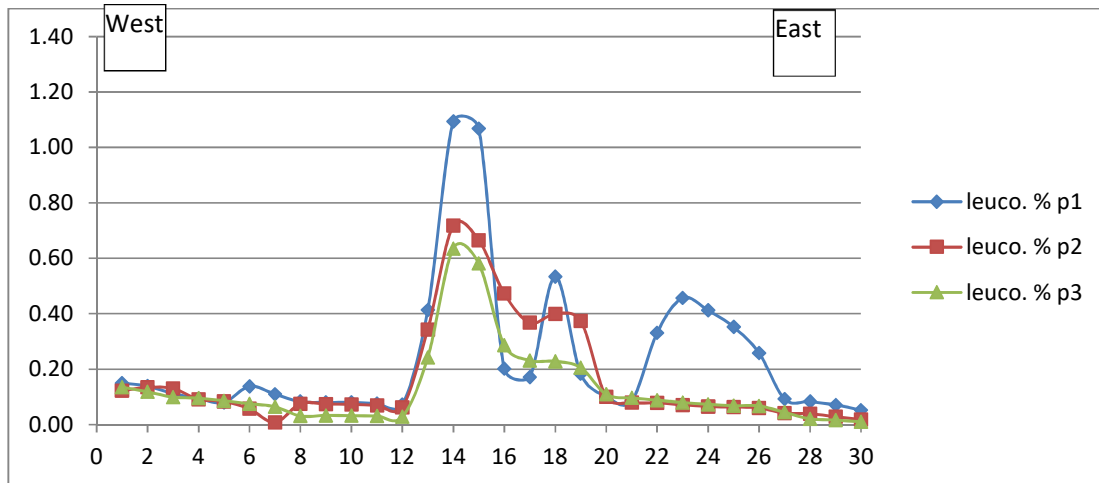


Fig. 9: lateral distribution of leucoxene.

The Non-opaque minerals

Rutile

Rutile is one of the three polymorphs of titanium dioxide, rutile, anatase and brookite. It is considered the most common form of TiO_2 in nature (Deer *et al.*, 1975). Hammoud (1966) classified the rutile in the Egyptian black sand into different classes, 2.9 wt.% opaque ilmenorutile, 4.2 wt.% ferriiferous rutile, 6.1 wt.% ex-translucent ilmenorutile, 19.8 wt.% secondary rutile and 67 wt.% translucent rutile.

Rutile has a wide range of magnetic susceptibilities. It concentrates in the low magnetic fields according to its iron content. Egyptian beach rutile is transparent, translucent and opaque. The Egyptian rutile particles appear under the binocular stereomicroscope as small prismatic euhedral to subhedral grains with red (Fig. 10a) to black color (Fig. 10b). Some rounded (Fig. 10c), discoidal grains (Fig. 10d) and oval shape (Fig. 10e) have colors varying from black, brown, red, and orange to yellowish, simple twinning was detected in some grains.

The Egyptian rutile and leucoxene (produced from the Egyptian black sand by Nuclear Materials Authority of Egypt) are used in the manufacture of welding electrodes. The production of both minerals is not sufficient for the local market. Rutile and leucoxene are imported from India and Australia.

In the first line (P1) rutile display content range from 0.001% to 0.326% with an average of about 0.064%, while, in the second line (P2) range from 0.001% to 0.283% with an average of about 0.077% and in the third line (P3) range from 0.002% to 0.233% with an average of about 0.049%.

Pure rutile grains were investigated under the Environmental Scanning Electronic Microscope (ESEM) and the elemental chemical compositions are shown that; pure rutile grain (Fig. 10f) and rutile grain (grey color) (Fig. 10g) with tantalite inclusion (light color) (Fig. 10h). The lateral distribution of rutile percentages is illustrated in (Fig. 11), and shows the high concentration at the central part of the studied area.

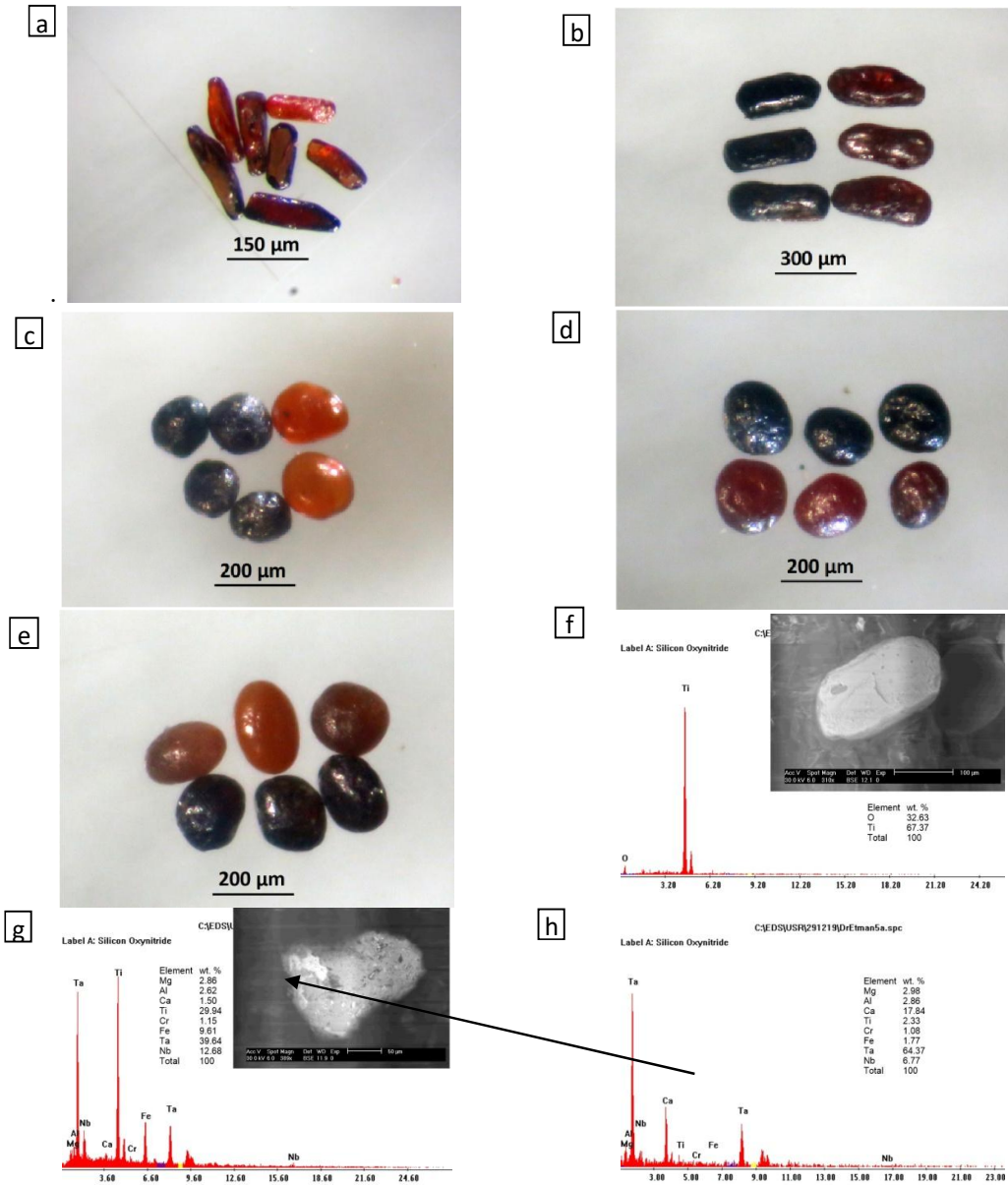


Fig. 10: Photomicrographs show: a) Red prismatic rutile, b) Red and black prismatic rutile, c) Red and black rounded rutile, d) Red and black discoidal and rounded rutile, e) Red and black oval rutile, f) EDX and BSE image of rutile, g) EDX and BSE image of rutile and h) EDX of tantalite inclusions in rutile grains.

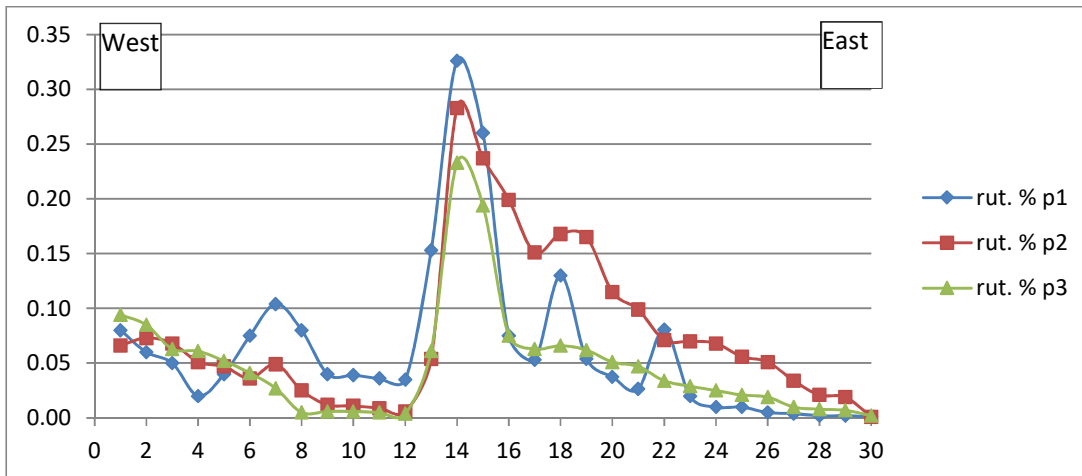


Fig. 11: Lateral distribution of rutile.

Garnet

The more common color for Egyptian black sand garnet is the pale pink. Garnet has moderate magnetic susceptibility which varies slightly according to variation in chemical composition (Milner, 1962).

Garnet crystallizes in the isometric system, at the Egyptian beach sand is mainly formed of angular to subrounded particles. Its hardness is about 7 (according to moh's scale of hardness) and its grain size is relatively coarser than the other economic minerals of the Egyptian beach sands. The recorded garnet varieties in the study area are moderately magnetic.

Garnet was recorded in the all studied samples as angular rose (Fig. 12a), red (Fig. 12b), subrounded to well rounded (Fig 12c). other garnet grains show different degree of inclusions which change its color from colorless to black (Fig. 12d) and (Fig. 12e) shows different colors of garnet grains.

In the first line (P1) garnet display content range from 0.041% to 2.505% with an average of about 0.452%, while, in the second line (P2) range from 0.011% to 0.814% with an average of about 0.165% and in the third line (P3) range from 0.015% to 0.811% with an average of about 0.150%. Garnet was separated at magnetic field strength 0.2A and 0.5A.

Pure garnet grains were investigated under the Environmental Scanning Electronic Microscope (ESEM) and the elemental chemical compositions are shown in Figures (12f, g &h). The analyzed garnet grains are represented mainly by almandine ($Fe_3Al_2Si_3O_{12}$), as a major component and many grain show different degrees of inclusions which ilmenite represented the main constituent (Fig. 12h) . The lateral distribution of garnet percentages illustrated in (Fig. 13) and show the high concentration at the central part of the studied area.

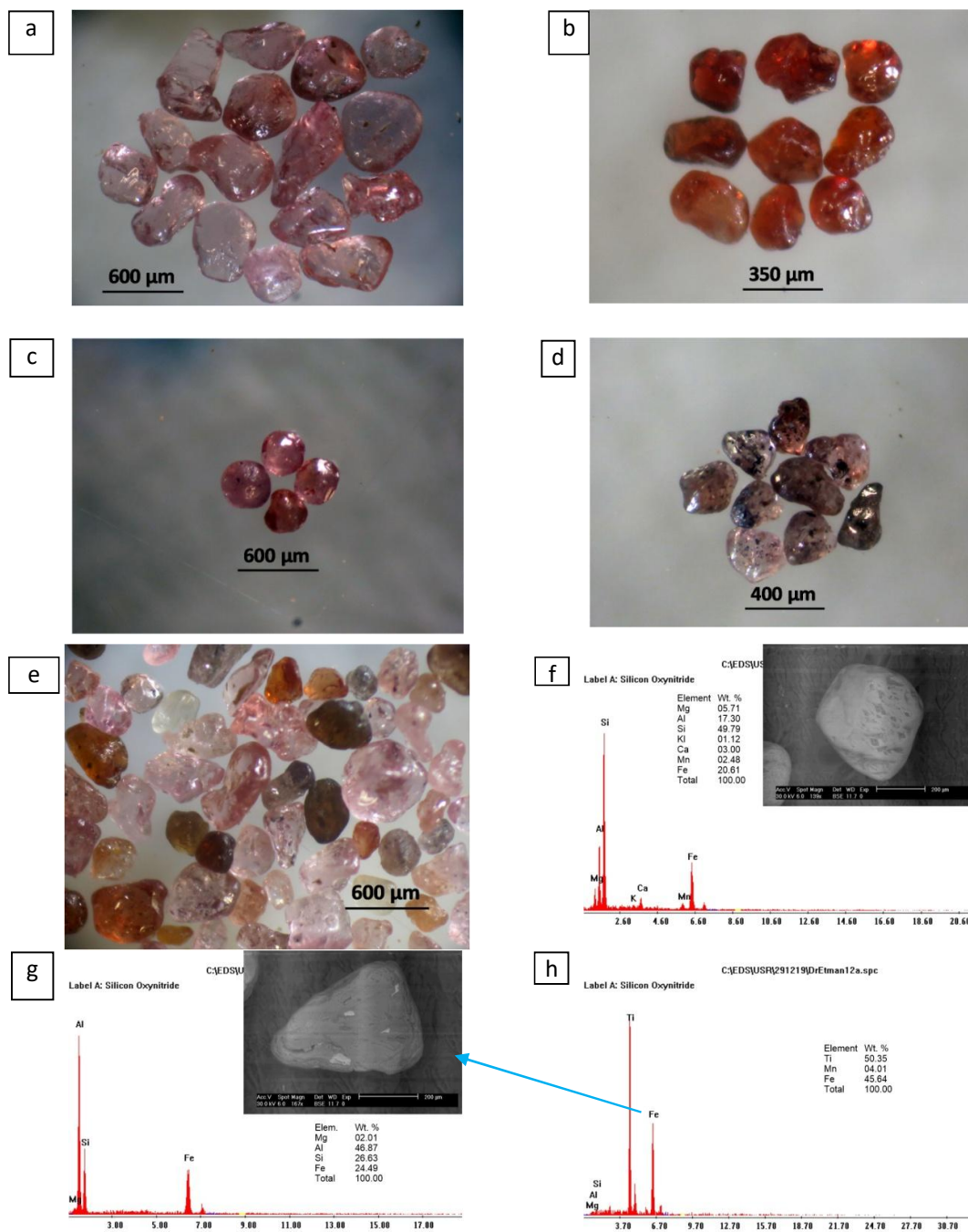


Fig. 12: Photomicrographs show: a) Rose garnet, b) Red garnet, c) rounded rose and red garnet, d) garnet with black inclusions, e) different colors of garnet grains, f) EDX and BSE image of almandine garnet, g) EDX and BSE image of almandine garnet with ilmenite inclusions and h) EDX of ilmenite inclusions in almandine garnet.

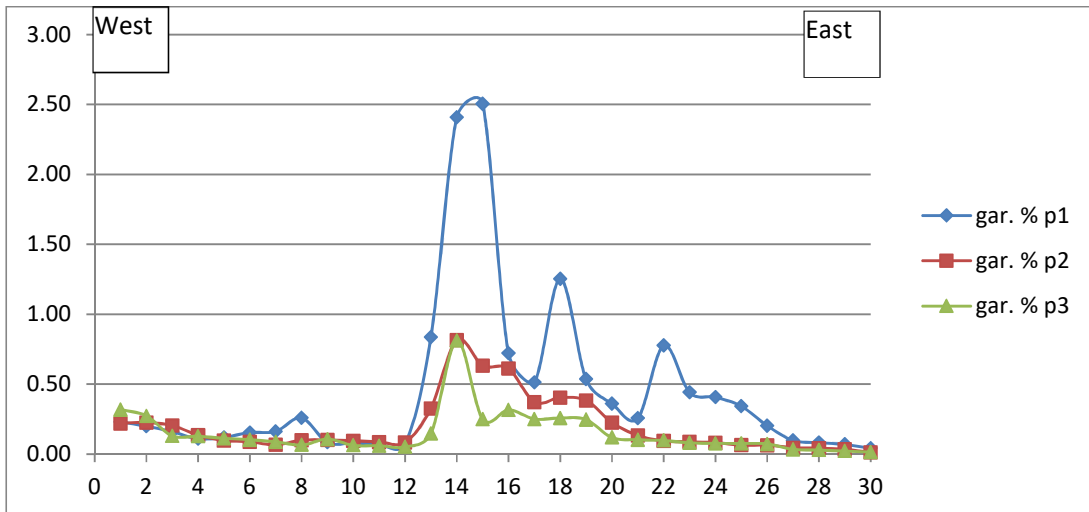


Fig. 13: Lateral distribution of garnet.

Staurolite ($Fe^{2+}_2 Al_9 O_6 (SiO_4)_4(O, OH)_2$)

Staurolite grains $(Fe, Mg)_2 (Al, Fe)_9 O_6 (SiO_4)(OOH)$ were separated at magnetic field strength 0.2A and 0.5A and were picked using binocular stereomicroscope. Barakat (2016) stated that: Staurolite represent about 3% of garnet concentrate and it has been used as an abrasive. Staurolite occur as yellow road like (Fig. 14a). Pure staurolite grains were investigated under the Environmental Scanning Electronic Microscope (ESEM) and the elemental chemical compositions are shown in figure (14b).



Fig. 14: a) Photomicrographs show: Yellow staurolite grains, b) EDX and BSE image of staurolite.

Zircon

Egyptian black sand zircon exhibits a peculiar behavior in regards to its magnetic susceptibility. This is due to the presence of inclusions which are different in quantity and in nature. Rittman and Nakhla (1958) classified the black sand zircon into, strongly magnetic (1 wt. %), moderately magnetic (8 wt. %) and non-magnetic (91wt. %).

The radioactivity of Rashid black sand zircon was studied previously by Gindy (1961), Meshref (1962) and El-Hinnawi (1964), they classified the zircon grains according to their radioactivity and remarked that the darker and / or zoned zircon are more radioactive than colorless zircon.

Zircon is mainly zirconium silicate with uranium, thorium, titanium and rare earth elements in minor quantities. The Egyptian black sand zircon was divided in to, the colorless water clear zircon which contains the lowest values of uranium and thorium (0.046 wt. % U_3O_8 and 0.02 wt. ThO_2) and constitute about 82.28 wt. % of the total zircon and the brown dark colored radioactive zircon which constitute about 17.72 wt. % of the total zircon (Dabbour, 1994).

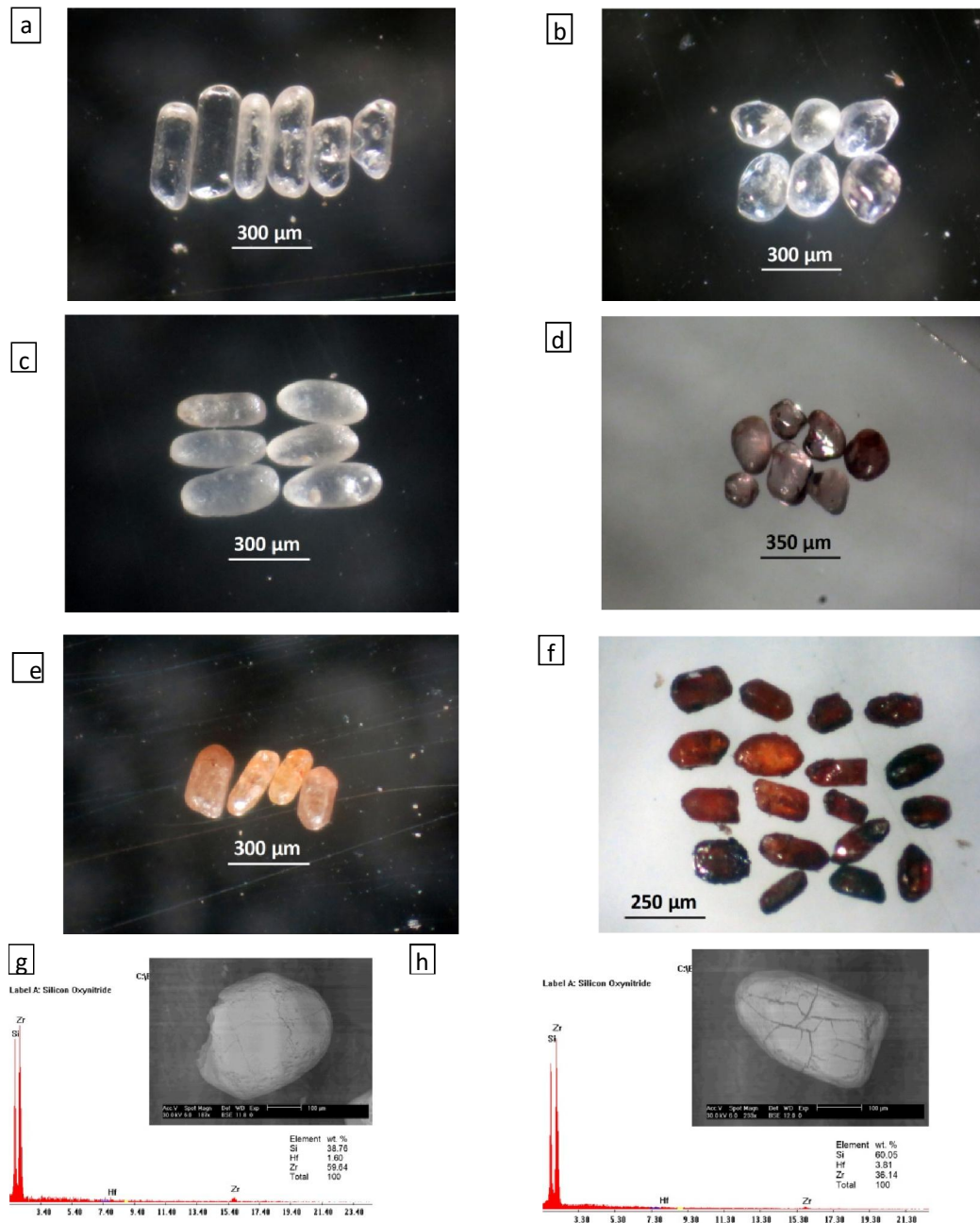


Fig. 15: Photomicrographs show: a) colorless prismatic zircon, b) colorless rounded zircon, c) white prismatic with rounded termination zircon, d) honey color zircon, e) yellow prismatic zircon, f) red prismatic zircon, g & h) EDX and BSE image of zircon.

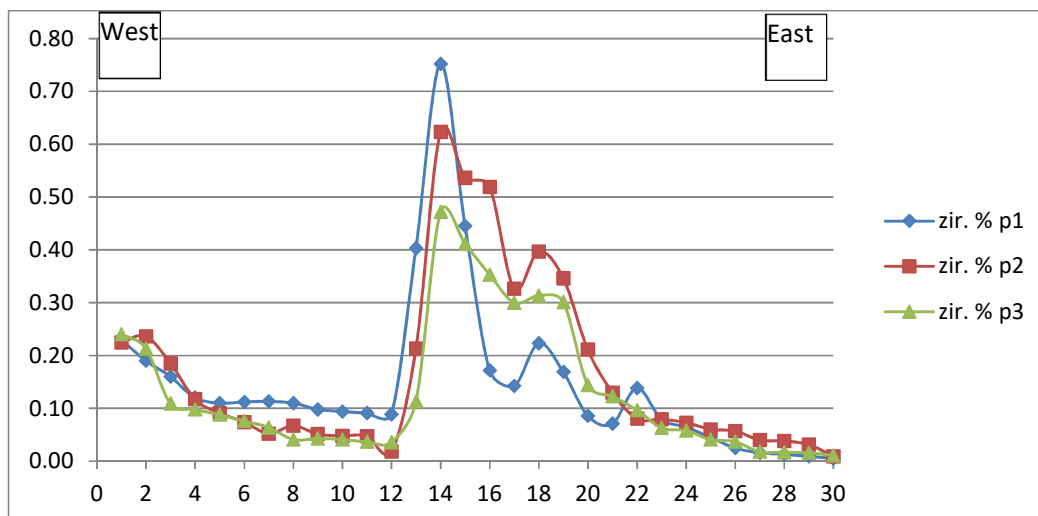


Fig. 16: lateral distribution of zircon.

Most of zircon grains have an euhedral external morphology. It was recorded as colorless short to long prismatic with or without bi-pyramid termination (Fig. 15a), colorless sub-rounded to rounded (Fig. 15b), white prismatic with smooth curved edges (Fig. 15c) and honey color (Fig. 15d). However, it is concentrated in both non-magnetic and magnetic fractions at 1.5A. Zircon separated in the nonmagnetic field 1.5A have long prismatic water clear color with vitreous luster. Armstrong (1922), Groves (1930), Poldervart (1955-1956) and Saxena (1966) stated that the water clear zircon grains in all types of rocks are nonmagnetic.

On the other hand, the magnetic zircon was recorded as reddish yellow and yellow prismatic (Fig. 15e) and red euhedral grains (Fig. 15f). The variation in the color of zircon may be attributed to the density of fine inclusions as well as the degree of iron oxides staining. Some inclusions may be due to iron ions that could penetrate from the original melt through zircon lattice during magmatic crystallization or from an outside source (Hassan 2005 and Surour *et al.*, 2003). These inclusions are considered as weak points which accelerate the disintegration of the grains (Carroll, 1953). Pure zircon grains were investigated under the Environmental Scanning Electronic Microscope (ESEM) and the elemental chemical compositions are shown in Figures (15g & h).

In the first line (P1) zircon display content range from 0.005% to 0.752% with an average of about 0.146%, while, in the second line (P2) range from 0.009% to 0.623% with an average of about 0.166% and in the third line (P3) range from 0.011% to 0.472% with an average of about 0.132%. The lateral distribution of zircon percentages illustrated in (Fig. 16), and show the high concentration at the central part of the studied area.

Monazite

Monazite is essentially an anhydrous orthophosphate of the cerium and lanthanum group of the rare earth elements which represented by cerium, lanthanum, praseodymium and neodymium which make up to 92 wt. % of Q the total rare earths. The yttrium group of rare earths together with minor amounts of Ca, Mg, Mn, Fe, Al, Zr, Be and Sn occur in substitution for Ce and La only in relatively small amounts. Both of huttonite (ThSiO₄) and brabantite {CaTh (PO₄)₂} are iso-structural with monazite and there may be continuous series between them with the coupled substitution, (Harlov *et al.*, 2007).

The Egyptian beach monazite occurs as very well-rounded grains, mostly taking the oval shape with high sphericity. It is free from inclusions and has colors varying from colorless to deep brown. Zaghoul and Kamel (1965) identified six color varieties of the Egyptian beach monazite, they are brown, yellowish brown, reddish brown, yellow, honey yellow and lemon yellow. They concluded that, the two principal colors of this mineral are the lemon yellow (59%) and the honey-yellow ones (25%). According to Milner (1962), monazite is weakly magnetic. Monazite is essentially a phosphate of rare earth mainly cerium, thorium and uranium in which thorium and yttrium substitute for cerium.

Their color ranges from colorless (Fig. 17a), lemon yellow (Fig. 17b), light red and deep red (Fig. 17c) to black which found in (Fig. 19d). They occur as accessory mineral in the fine and very fine sand fractions. It was separated at magnetic field strength 0.5A and 1.0A. Monazite exhibits shape varies between rounded, discoidal, oval and prismatic.

In reality, monazite technically four different minerals technically, but because of a lack of great differences between them they are referred to as one mineral monazite. The four monazites have differences in the percentages of their chemical constituents. Their differences are reflected in their respective names (Van Emden *et al.*, 1997):

1. (Ce)-Monazite: (Ce, La, Nd, Th, Y)PO₄
2. (La)-Monazite: (La, Ce, Nd)PO₄
3. (Nd)-Monazite: (Nd, La, Ce)PO₄
4. (Sm)-Monazite: (Sm, Gd, Ce, Th)PO₄

Pure monazite grains were investigated under the Environmental Scanning Electronic Microscope (ESEM) and the elemental chemical compositions are shown in figures (19e & f). All monazite of the studied sediments belongs to (Ce)-Monazite.

In the first line (P1) monazite display content range from 0.000% to 0.013% with an average of about 0.0044%, while, in the second line (P2) range from 0.0001% to 0.019% with an average of about 0.007% and in the third line (P3) range from 0.0001% to 0.014% with an average of about 0.006%. The lateral distribution of monazite percentages illustrated in (Fig. 18), and show the high concentration at the central and the west parts while the lowest concentration located in the east part of the studied area.

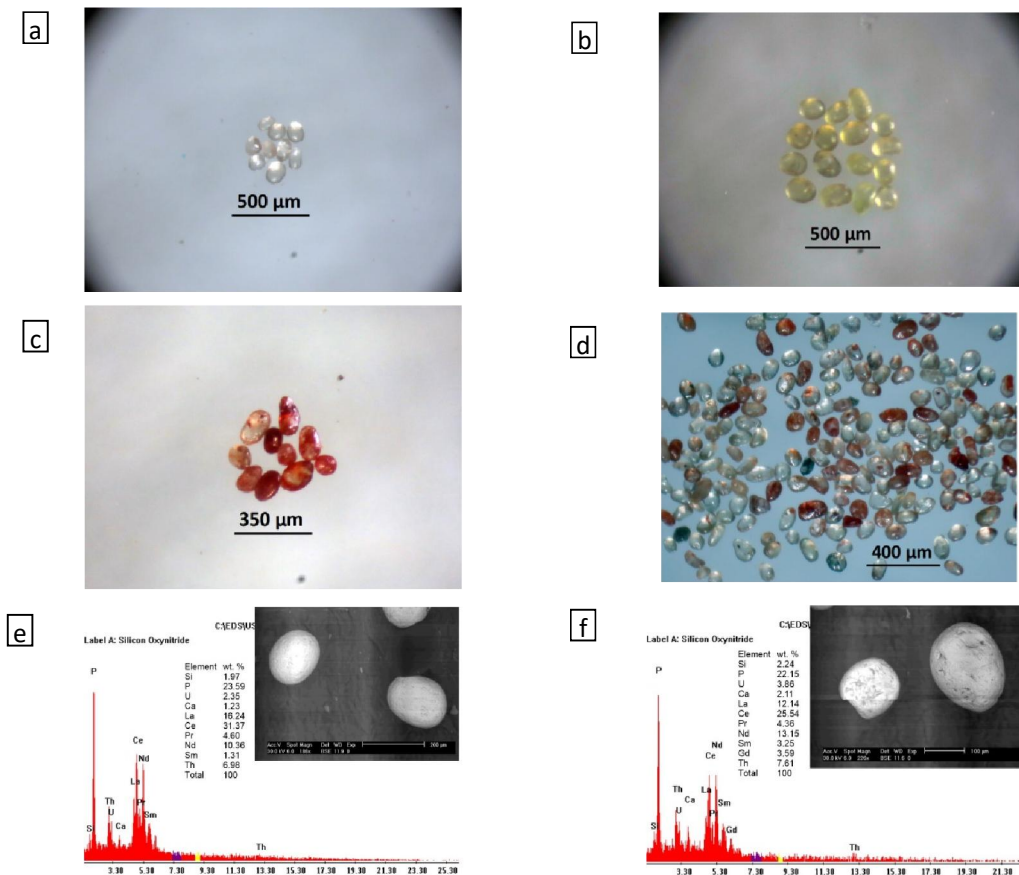


Fig. 17: Photomicrographs show: a) colorless rounded monazite, b) lemon yellow monazite, c) red monazite, d) different colors and shapes of monazite grains, e & f) EDX and BSE image of monazite.

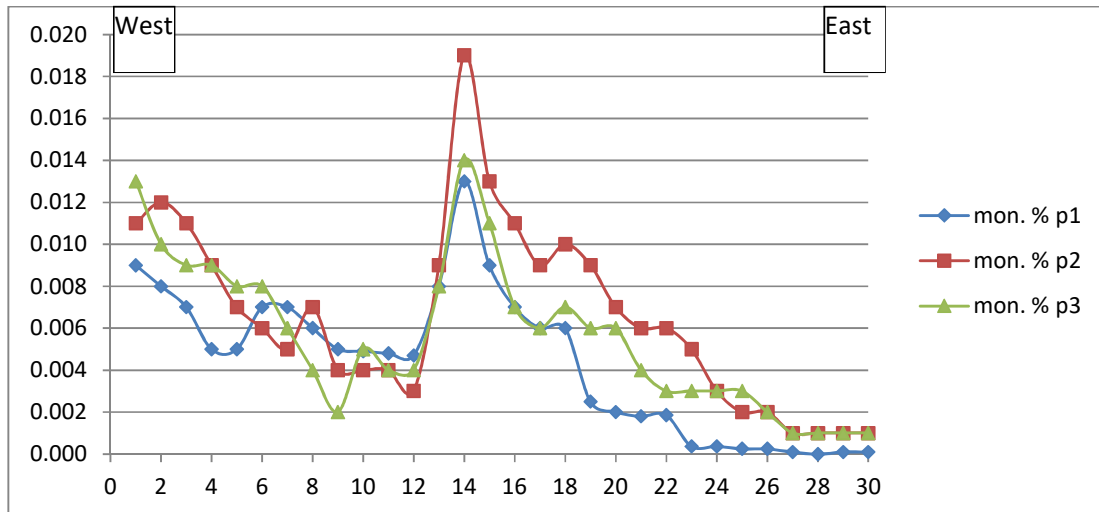


Fig. 18: Lateral distribution of monazite.

Titanite (Sphene) (CaTiSiO₅)

Titanite is more common in all samples of the studied sediments. Its color varies from yellowish to brownish yellow with vitreous luster (Fig. 19a). Titanite mineral grains are subhedral to anhedral grains with imperfect cleavage. Titanite was separated at magnetic field strength 1.0A and less common in 0.5A. Pure titanite grains were investigated under the Environmental Scanning Electronic Microscope (ESEM) and the elemental chemical compositions are shown in Figure (19b).

In the first line (P1) titanite display content range from 0.000% to 0.060% with an average of about 0.0092%, while, in the second line (P2) range from 0.001% to 0.024% with an average of about 0.010% and in the third line (P3) range from 0.001% to 0.015% with an average of about 0.007%. The lateral distribution of monazite percentages illustrated in (Fig. 20) and show the high concentration at central part of the studied area.



Fig. 19: a) Photomicrographs show: yellowish to brownish yellow titanite.

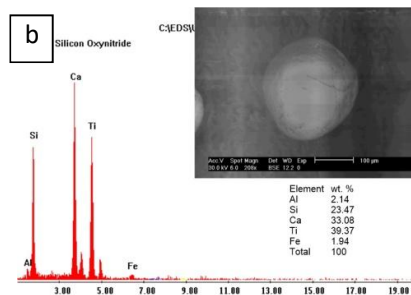


Fig. 19: b) EDX and BSE image of titanite.

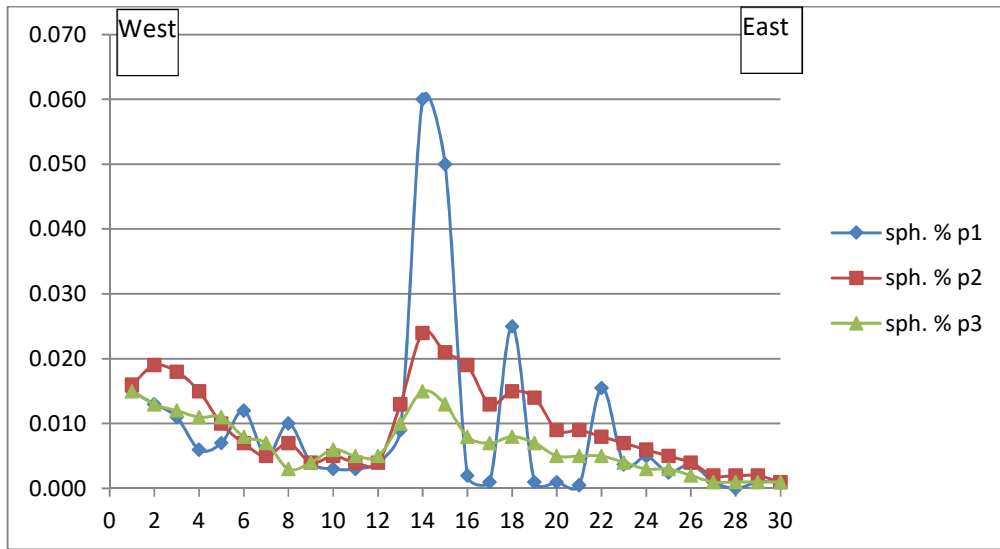


Fig. 20: Lateral distribution of titanite.

Accessory minerals

Gold (Au)

Hammoud and Khazback (1984), and El-Gemmizi (1985) detected the presence of gold particles in the beach sands east and west of Rashid mouth. They concluded that, the gold particles ranging from 0.57 g/ton to 2 g/ton.

In our study, the shape of these grains is irregular, oval and rounded to sub-rounded discoidal grains (Fig. 21a) and elongated grains (Fig. 21b). Gold grains are clean, uncoated and not tarnish, and golden yellow color particles with brilliant metallic luster. Pure gold grains were investigated under the Environmental Scanning Electronic Microscope (ESEM) and the elemental chemical compositions are shown in figures (21c & d).

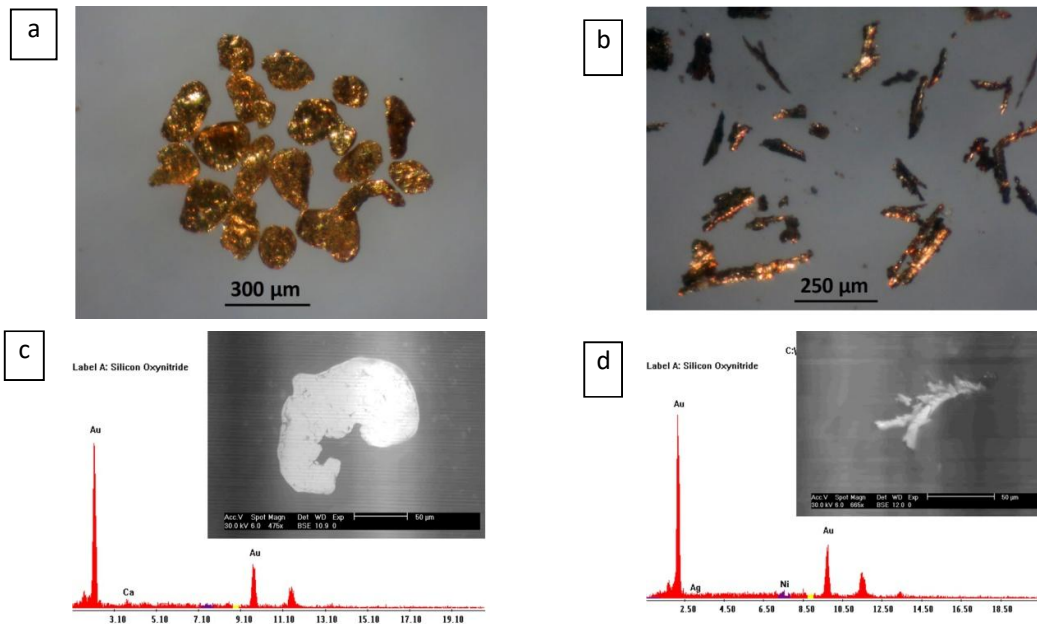


Fig. 21: Photomicrographs show: a) Discoidal Gold, b) road like shape gold, c) EDX and BSE image of native discoidal gold and d) EDX and BSE image of native road like shape gold.

Alumina minerals

Aluminum is a relatively soft, nonmagnetic, ductile and malleable silvery metal. It is the most common metal present in the Earth's crust and the third most common element (after oxygen and silicon). It is moderately reactive and never found in pure form in nature. It exhibits grayish-white color, metallic luster and massive grains with platy or scaly aggregates (Fig. 22a). Pure aluminum grains were investigated under the Environmental Scanning Electronic Microscope (ESEM) and the elemental chemical compositions are shown in figure (22b). Aluminum has hundreds of uses, from aircraft and vehicle parts to building material, beverage cans, wrapping foil and just about any applications where a lightweight metal is needed.

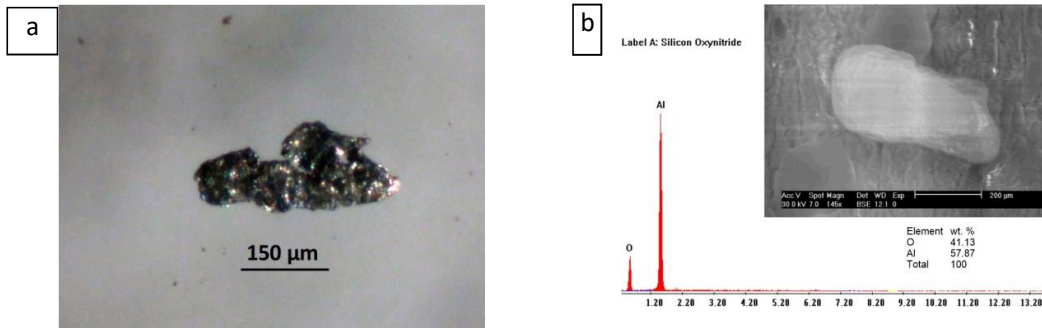


Fig. 22: a) Photomicrographs show: Alumina mineral, b) EDX and BSE image of Alumina mineral.

Chromite $FeCr_2O_4$

Chromite is the main ore of chromium and has a wide range in industrial uses. It is used as a refractory material due to its high heat stability. Chromite usually occurs as well formed octahedron crystals. It was separated at 0.2A and 0.5A using Frantz Isodynamic Separator. Its color varies from black to brownish black with metallic luster (Fig. 23a). Pure chromite grains were investigated under the Environmental Scanning Electronic Microscope (ESEM) and the elemental chemical compositions are shown in figure (23b).

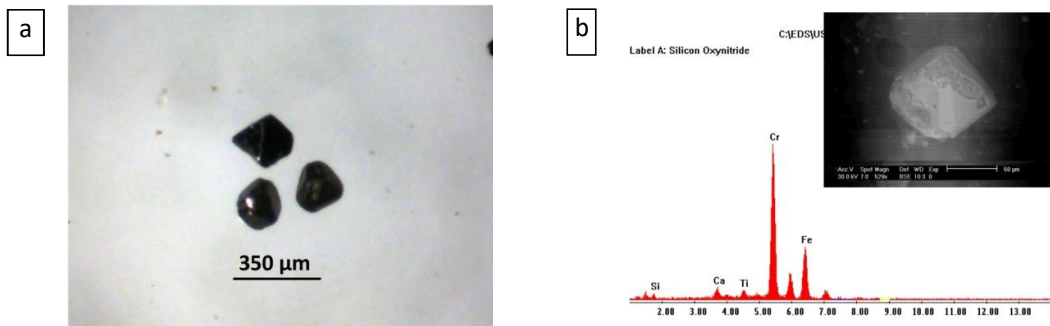


Fig. 23: a) Photomicrographs show: Octahedron chromite, b) EDX and BSE image of muscovite.

Pyrite (FeS_2)

Pyrite is one of the few minerals that are produced by biological micro-environmental systems. It is a common sulphide mineral together with chalcopyrite. It has well developed rounded shape with two variant colors, as were as golden yellow or shiny brassy yellow, and blue (Fig. 24a and b respectively). Pure pyrite grains were investigated under the Environmental Scanning Electronic Microscope (ESEM) are shown in (Fig. 24c) which its EDX shows the pure composition. Pyrite was separated at magnetic field strength 1.5A using the Frantz Isodynamic separator.

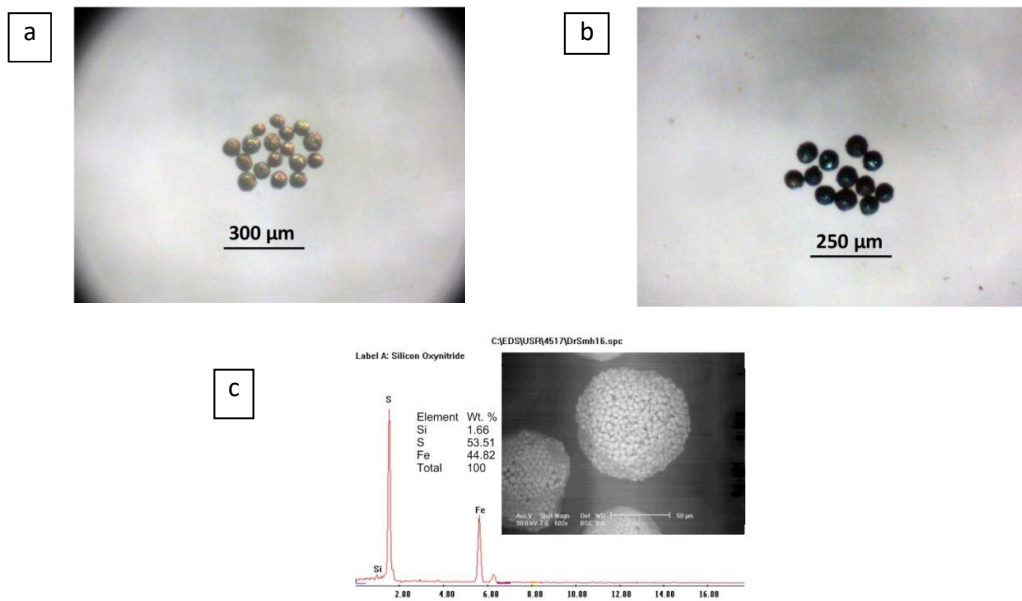


Fig. 24: a): Photomicrographs show: Golden yellow pyrite, b): Photomicrographs show: Blue pyrite, c): EDX and BSE image of pyrite.

Cassiterite (SnO_2)

The majorities of cassiterite grains are translucent to opaque and have colours varying from colourless, brown, dark brown, grey, black and red (Fig. 25a & b).

Cassiterite (SnO_2) has been the chief tin ore throughout ancient history and remains the most important source of tin today. In its purest form cassiterite contains 78.6 wt. % tin, but when contaminated with impurities the tin content varies between 73 and 75 wt. %. Cassiterite typically contains tantalum and niobium and generally appreciable amount of ferrous or ferric iron and smaller amounts of Mn, Ti and Sc. (Deer *et al.*, 1975).

Cassiterite, also called tinstone, is a heavy mineral of great economic importance as tin source. Pure cassiterite has the following properties (Elsner 2010): Formula SnO_2 , 78.8 % by mass Sn and 21.2 % by mass O_2 . In cassiterite, Sn can be replaced by Fe at a ratio of 1:6 as well as by Nb and Ta to a ratio 1:30. Other frequently occurring trace elements are Ti, Li, Sc, Zn, Fe, W and Mn.

The percentages of cassiterite and gold are considered negligible in the original raw sands, they could be recovered as a profitable by-product during the industrial exploitation of the huge reserve of the Egyptian black sands.

Cassiterite mineral is mainly used for extraction the metal tin and as almost the only tin mineral of economic importance. Tin is silvery white, very inert, and thus singularly suitable for protection against corrosion. Tin also used for, alloys production, soldering tin, opaque white glazed, as a stabilizer in PVC beside soap (SnCl_4), toothpaste (SnF_2), tin cans (steel plated with tin), electronic devices and as a polishing compounds.

Pure cassiterite grains were investigated under the Environmental Scanning Electronic Microscope (ESEM) and the elemental chemical compositions are shown in Figure (25c & d).

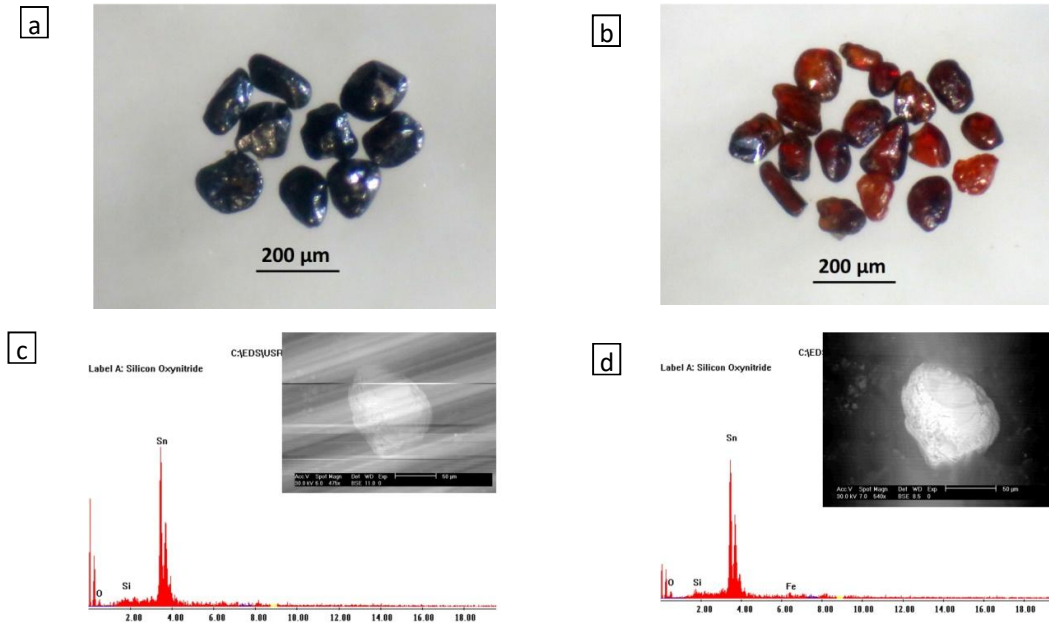


Fig. 25: Photomicrographs show: a) Black cassiterite, b) Red cassiterite, c & d) EDX and BSE image of cassiterite.

Apatite $\text{Ca}_5(\text{PO}_4)_3\text{F}$

Apatite is the most common phosphate mineral, representing the main source of phosphorus required to plants. Furthermore it represents the main component of the bones and teeth of most animals, including humans. It was recorded in the studied samples as wedge and irregular shape with brown color (Fig. 26a). Pure apatite grains were investigated under the Environmental Scanning Electronic Microscope (ESEM) and the elemental chemical compositions are shown in Figure (26b).

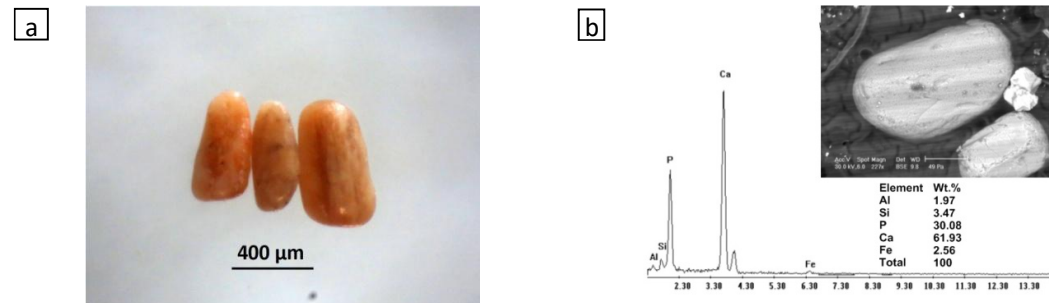


Fig. 26: a) Photomicrographs show: apatite, b) EDX and BSE image of apatite.

Gahnite (ZnAl_2O_4)

Gahnite, is a rare mineral belonging to the spinel group. It forms octahedral crystals which may be green, blue and yellow (Fig. 27a). Trace spherical grains of gahnite were picked under the stereo binocular-microscope. Pure gahnite grains were investigated under the Environmental Scanning Electronic Microscope (ESEM) and the elemental chemical compositions are shown in (Fig. 27b).

Kyanite Al_2SiO_5

This mineral is one of the kyanite, sillimanite, andalusite metamorphic mineral group. Kyanite show blue, white, rarely green, gray, yellow, pink, orange, and black color, transparent to translucent (Fig. 28a), The crystal habit ranges from columnar; fibrous; bladed, vitreous to pearly luster, and perfect cleavage. Pure kyanite grains were investigated under the Environmental Scanning Electronic Microscope (ESEM) and the elemental chemical compositions are shown in figure (28b). Kyanite is commonly found in aluminium-rich metamorphic pegmatites and/or sedimentary rock. Kyanite in metamorphic rocks generally indicates pressures higher than 4 kb.

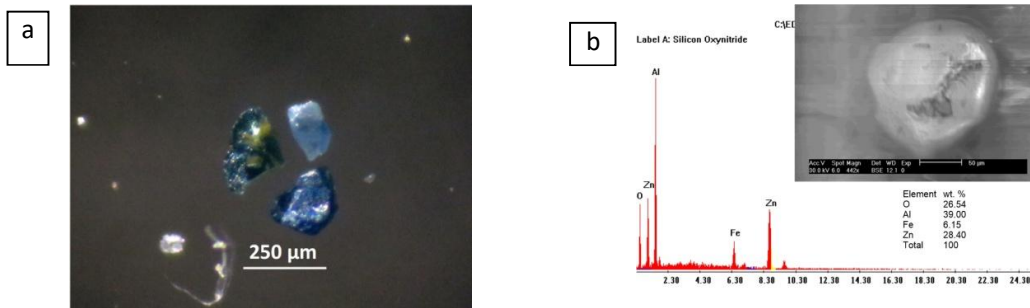


Fig. 27: a) Photomicrographs show: gahnite. b) EDX and BSE image of gahnite.

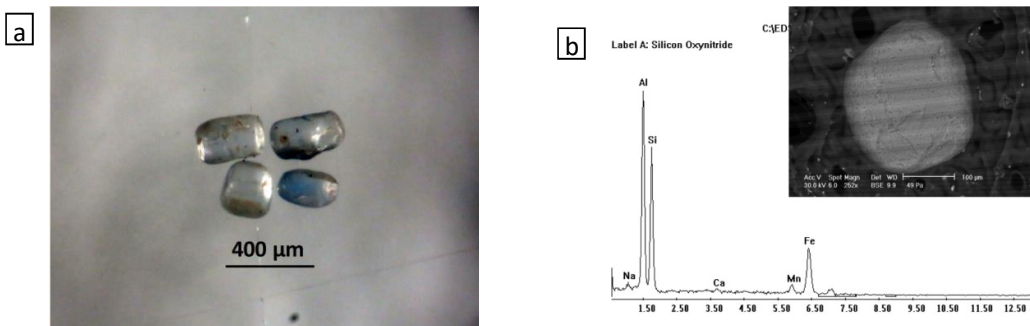


Fig. 28: a) Photomicrographs show: kyanite, b) EDX and BSE image of kyanite.

Green Silicates

The green silicates are common minerals in these sediments, and separated using heavy liquid bromoform (sp. gr. 2.86 gm/cm³). It is mainly concentrated in the first magnetic fraction 0.2A and the rest found in 0.5A and decreases with increasing of magnetic field strength.

This mainly fraction includes silicate with sheet structure as mica including muscovite and biotite, silicate with single chain pyroxene group comprising five important minerals (bronzite, hyperthene, diopsed, hedenbergite, augite, aegirine, and jadite) which are altered to carbonates or chlorite minerals, and double chain amphiboles group which contain anorthophyllite, tremolite, actinolite, cummingtonite, hornblend, glaucophane, rebekite, and arfvedsonite, which are altered to serpentine or chlorite or carbonate. This is in addition to silicate with isolated tetrahedral as olivine group, and less common kyanite, sillimanite, andalusite, and staurolite, and isolated double tetrahedral epidot group.

4. Conclusion

The results revealed that, the total heavy minerals content in the studied area are restricted mainly in the central and western parts, while the eastern part show low content. This increasing is mainly related to: -

- 1- The old extinct branches (Bolbinitic, Saitic and Sebennitic) (Fig. 2) in the central part.
- 2- Rashid branch in the western delta receive today most of water as it has less meandering and more bifurcates into the delta fan compared with Dumyat branch.

The total heavy minerals range from 1.153% to 55.897% with an average of about 11.208% for line P1, range from 0.770% to 48.510% with an average of about 9.223% for line P2 and range from 0.690% to 35.640% with an average of about 8.728% for line P3. These results revealed that, the average of total heavy minerals decreases south ward.

The identified heavy economic minerals in the studied area can be classified into two main groups: -

- 1- Opaque minerals as: magnetite with an average of about 0.542% for line P1, 0.612% for line P2 and 0.600% for line P3. Ilmenite with an average of about 1.936% for line P1, 1.387% for line P2 and 1.394% for line P3. Leucoxene with an average of about 0.239% for line P1, 0.165% for line P2 and 0.130% for line P3.
- 2- Non-opaque minerals as: rutile with an average of about 0.064% for line P1, 0.077% for line P2 and 0.049% for line P3. Garnet with an average of about 0.452% for line P1, 0.165% for line P2 and 0.150% for line P3. Zircon with an average of about 0.146% for line P1, 0.166% for line P2 and 0.132% for line P3. Monazite with an average of about 0.0044% for line P1, 0.0070% for line P2 and 0.0060% for line P3. Titanite with an average of about 0.0092% for line P1, 0.010% for line P2 and 0.007% for line P3.
- 3- Accessory minerals as: gold, hematite, chromite, pyrite, cassiterite, apatite, gahnite and kyanite.

References

- Abu Diab, A.A., 2002. Sedimentological studies and economic evaluation of the coastal sand dunes between El Geddia and Idku, Rosetta. Egypt. Unpub. M.Sc. Thesis, Fac. Sci., Mansoura Univ., Mansoura, Egypt.
- Ali, M.M., K.F. Mahmoud, and A.A. Dewedar, 2003. Suggested method for dissolution of Egyptian beach ilmenite. *Sci. J. Fac. Sci., Minufiya Univ.*, Vol, XVII (2003:309-331).
- Arafa, E.H.M., 1990. mineralogical and sedimentological studies of some sediments from Egypt and Sudan. Ph. D. thesis, Fac. of Sci. Cairo Univ., Egypt.
- Armstrong, P., 1922. Zircon as criterion of igneous or sedimentary and metamorphic. *Amer.*, Vol. 5(4): 395.
- Bailey, S.W., E.N. Cameron, H.R. Spedden, and R.J. Weege, 1956. The alteration of ilmenite in beach sands. *Econ. Geol.*, 51: 263-279.
- Ball, J., 1942. Egypt in the classical geographers. *Geol. Surv. Egypt*.
- Barakat, M.G., 2016. Evaluation and mineralogy of beach economic minerals especially ilmenite for the top meter in the Egyptian black sand, east Rosetta, Egypt. Ph. D. Thesis, Fac. Sci. Zagazig university, Egypt, 284.
- Basta, E.Z., 1972. Different types of ilmenite-magnetite intergrowths and their origin. *Bull.; Fac. Sci.; Cairo University*, 44: 195-212.
- Carroll, D., 1953. Weatherability of zircon. *J. Sed. Pet.*, 23: 116.
- Costa, J.E., K.R. Spicer, R.T. Cheng, F.P. Haeni, N.B. Melcher, E.M. Thurman, W.J. Plant, and W.C. Keller, 2000. Measuring stream discharge by non-contact methods: A proof-of-concept experiment. *Geophysical Research Letters*, 27(4):553-556.
- Dabbour, G.A., 1994. The Egyptian placer deposits-a potential source for Nuclear Raw Materials, Second Arab Conference on the peaceful uses of Atomic Energy, Cairo, 5-9 Nov. part 11: A, Scientific Paper.
- Dabbour, G.A., 1997. Mineralogical study on the opaque minerals and secondary rutile from the Egyptian black sand. *Proceeding of the Egyptian Academy of Science*. V. 47.

- Dabbour, G.A., T.M. Labib, and A.F. Bakhit, 1999. El Burullus sand dunes belt, a real black sand deposits, First Seminar on Nuclear Raw Materials and other Technology, 1-3 Nov.48 p.
- Deer, W.A., R.A. Howie, and J. Zussman, 1975. An introduction to the rock forming minerals. Longman group Ltd., London, 528.
- Dewedar, A.A.M., 1998. Comparative studies on the heavy minerals in some black sands from Sinai and east Rosetta, with contribution to the mineralogy and economics of their garnets. Unpubl. Ph.D. Thesis, Fac. Sci., El Menoufia Univ., Shibin El-kom, Egypt.
- El Alfi, S.M., 2019. Inferred resources of heavy economic minerals in West El Burullus area, Egypt. *Journal of Sedimentological society of Egypt*, 24:129-147.
- El-Afandy, A.H., M.I. Moustafa, H.A. El Nahas, A.A. Abdou, and M.G. Barakat, 2016. Geomorphology and Mineralogy of the top meter Black Sands North West of El-Burullus Lake, Kafr Al-Sheikh Governorate, Egypt. *Al Azhar Bulletin of Science*, 27(2):65-72.
- El-Azab, A.I., 2006. Morphological and environmental study of Abu Qir- Rafah coastal plain with emphasis the beach black sand, Egypt. Ph. D. Thesis. Fac. Sci., Ain Shams University, Cairo.
- El Azab, A., S.M. El Alfi, and H.H. Ali, 2018. Mineralogy and Radioactivity of the Southern Part of Nasser Lake sediments, Egypt. *Al-Azhar Bulletin of Science*, 29(2):143-163.
- El Azab, A., S.M. El Alfi, and H.H. Ali, 2019. Economic Heavy Minerals Evaluation of Damietta Harbor Channel Sediments, Egypt. *Journal of Sedimentological society of Egypt*, 24:43-61.
- El Balaksky, S.S., 2003. Mineralogical studies for the economic minerals in the sand dune belts at Baltim area. Unpub. Ph D. Thesis. Fac. Sci. Ain Shams Univ., Cairo, Egypt.
- El-Bokel, F.M., 1984. Technical & Economic aspects for utilization of the Egyptian ilmenite in oil well drilling fluids. *Annals Geol. Surv.*, Egypt, vol. VXXV, 1-23.
- El-Gemmizi, M.A., 1985. Note on the occurrence of gold and cassiterite in the Egyptian beach placer deposits. *Econ. Geol.*, 80: 769-772.
- El-Hadry, A.F., 1998. Geological, sedimentological and radiometric studies on the black sand deposits, west Rosetta beach with emphasis on the heavy economic minerals, Unpub. Ph D. Thesis, Fac. Sci., Cairo Univ. Cairo, Egypt.
- El-Hinnawi, E.E., 1964. mineralogical and geochemical studies on Egyptian (U.A.R) black sands. *Beitrag Zur Mineralogie and Petrographie*. 9: 519-532.
- El-Kammar, A.A., A.A. Ragab, and M.I. Moustafa, 2010. Geochemistry of Economic Heavy Minerals from Rosetta Black Sand of Egypt. *Journal of KAAL: Earth Science, Kingdom of Saudi Arabia*, 22(2): 1-25.
- El Rakaiby, M.L., 2000. Utilization of remote sensenig investigation and monitoring the economic black sand along Rashid and Domiat coast, Egypt.
- El Rakaiby, M.L., and N. Attia, 2004. Morphological and geological classification of the Egyptian northern coastal environment using space image technology. *Bull. De la societe de geographic d’Egypt*, 77 (in press).
- Elsner, H., 2010. Heavy minerals of economic importance. Assessment manual, Faculty of Geosciences of the University of Hannover: 218, 31 Fig. 125 Tab.
- Flinter, B.H., 1955. A magnetic separation of some alluvial minerals in Malaya, *Amer. Miner.*, 44(7-8): 751.
- Folk, R.L., 1980. Petrology of sedimentary rocks. Univ. Texas, Hemphill, Pup. Co., Austin, Texas, USA.
- Gindy, A.R., 1961. Radioactivity of monazite, zircon and radioactive black grains in black sands of Rosetta, Egypt, *Econ. Geol.*, 56: 436- 441.
- Groves, A.W., 1930. The heavy minerals suite and the correlation f the granites of northern Brittany, The channel Islands, and the cotentin, *Geol. Mag.*, 67: 240.
- Hammoud, N.S., 1966. Concentration of monazite from Egyptian black sand, employing industrial techniques, Unpub. M. Sc. Thesis, Fac. Sci., Cairo Univ.
- Hammoud, N. S., 1973. Phisical and chemical properties of some Egyptian beach economic minerals in relation to their concentration problems. Unpub. Ph. D. Thesis, Fac. Sc. Cairo Univ., Cairo, Egypt.
- Hammoud, N.S. and A.E. Khazback, 1984. Traces of native gold particles in Egyptian northern beach heavy minerals deposits. *Egypt: Jour. Geol.*, 28: 79-82.

- Hany A.S., M.R. Atta, A.A. Bakhit, H.M. Diab, A.A. El Hagg and Samah Dahy, 2019. Natural Radioactivity Assessment and the associated Radiological Hazards for Beach Sand, Baltim area, Egypt. *Al-Azhar Bulletin of Science*, 30(1): 37-47
- Harlov, D.E., R. Wirth, and C.J. Hetherington, 2007. Replacement of monazite by a huttonite component: nature and experiment. *Am. Min.*, 92: 1652-1664.
- Hassaan, A.H.A., 2005. Evaluation of the heavy minerals in the coastal sand dunes, East Sabkhit Al-Tinna, North Sinai, Egypt. Ph. D. thesis, Fac., of Sci., Ain Shams Univ.
- Ibrahim, M.I.M., 1995. Investigation of physical properties of zircon and rutile to prepare high purity mineral concentrates from black sand deposits. Unpub. M.Sc. Thesis, Mansoura Univ., Mansoura, Egypt.
- Keller, E.A., 2000. Environmental geology. 8th ed. United States of America.
- Kuenan, 1962. Nile sediments in marine geology: J. Willey.
- Mansour, S.M.M., 2009. Geology, Mineralogy and Radioactivity studies on Nuweibi area, Central Eastern Desert, Egypt. M. Sc. thesis, Fac., of Sci., Benha University.
- Meshref, W.M., 1962. Mineralogical and radiometric study for black sands deposits on the Mediterranean coast, Unpub. M.Sc. Thesis, Fac. Sci., Ain Shams Univ., Cairo, Egypt.
- Milner, H.B., 1962. Sedimentary petrography. V, II, George Allen & Unwin, Ltd., London, 15-205.
- Mohamed, E., 1987. Mineralogical studies for some quaternary sediments in northern Sainai Unpub. M.Sc. Thesis, Fac. Sci., Suze Canal Univ., Suze, Egypt.
- Mohamed, S.S.M., 1998. Radioactivity and mineralogic studies on wadi Abu Dabbab alluvial deposits, Central Eastern Desert, Egypt. M. Sc. Thesis, Fac. of Sci., Ain Shams Univ. 204p.
- Moustafa, M.I., 2010. Mineralogical characteristics of the separated magnetic rutile of the Egyptian black sands. *Resource geology*, 60(3): 300-312.
- Poldervart, A., 1955. Zircon in sedimentary rocks. *Am. J. Sci.*, 433: 461.
- Poldervart, A., 1956. Zircon in igneous rocks. *Am. J. Sci.*, 254: 554.
- Rabie, S.I., G.A. Dabbour, A.M. Kafafy, and A.A. Nigm, 1995. Ground geophysical investigations of the total heavy minerals in Abu Khashaba black sands, Rosetta, Egypt. *Proc. Egypt. Acad. Sci.*, 45:101-119.
- Ragab, H., A.H. El Afandy, M. Khalil, and A. Yousry, 2017. Inferred Resources and Environmental Impact of the top meter Black Sands in the coastal area of Mediterranean Sea between Damietta Sea Port and Gamasa City, Egypt. *Al Azhar Bulletin of Science*, 28(1): 1-13.
- Rittman, A. and F.M. Nakhla, 1958. Contribution to the study of Egyptian black sands. *Jour. Chem. V. 1*: 127-135.
- Sadek, H.S., S.A. Soliman, H.M. Abdel hadi, and A.A. Hosni, 1988. Geophysical exploration of the black sands of Abu Khashaba beach. Rosetta, Egypt. Internal Rep. (Confidential), N.M.A., Cairo, Egypt.
- Samy, Y. and A. El-Gohary, 2013. Heavy Minerals Pattern and Indices as a Guide for Provenance and Transportation of Beach Sands along the Northern Sinai Coast, Egypt. *Journal of Applied Sciences Research*, 9(11): 5656-5664, 2013 ISSN 1819-544X.
- Saxena, S.K., 1966. Evaluation of zircon in sedimentary and metamorphic rocks. *J. Sed.*, 2: 33.
- Summerfield, M.A., 1991. Tectonic geomorphology. *Progress in physical geography. Jun*; 152: 193-205.
- Surour, A.A., A.A. El-Kammar, E.H. Arafa, and H.M. Korany, 2003. Dahab stream sediments, south eastern Sinai, Egypt: a potential source of gold, magnetite and zircon. *Journal of Geochemical exploration*, 77: 25-43.
- Teufer, G. and A.K. Temple, 1966. Pseudorutile - a new mineral intermediate between ilmenite and rutile in the alteration of ilmenite. *Nature*, 211:179-181.
- Van Emden, B., M.R. Thornber, J. Graham, and F.J. Lincoln, 1997. The incorporation of actinides in monazite and xenotime from placer deposits in Western Australia.- *The Canadian Mineralogist*, 35: 95 – 104, 5 fig., 4 tab.; Ottawa, ON.
- Ward, J. and R. Towner, 1985b. : Japan.- in: UNESCAP & BMR: Mineral sands in Asia and the Pacific.- Mineral concentrations and hydrocarbon accumulations in the ESCAP region, 4: 76– 80, 1 fig., 4 tab.; w/o place, Australia.
- Wassef, S.N. and M.A. Mikhail, 1981. Distribution and mineralogy of ilmenite and other accessory minerals in the beach sands of west Rosetta, Egypt. *Desert Instit. Bull., A.R.E.*, 31(1-2):17-29.

- Wiegel, R.L., 2009. The Nile River Delta coast and Alexandria seaport, Egypt. A brief overview of history, problems and mitigation. University of California, Berkeley, 16.
- Yousria Samy and E. Amr, 2013. Heavy Minerals Pattern and Indices as a Guide for Provenance and Transportation of Beach Sands along the Northern Sinai Coast, Egypt.
- Zaghloul, Z.M. and K. Kamel, 1965. The mineralogical and Petro – graphical features of monazite from the black sands of Rosetta. *J. Geol. U.A.R.*, 9(1): 17 - 31.